Final Examination

MSc SENSE

Voltag Droop Control Design for DC Microgrids

Master Thesis

Author: Doru Bogdan Bolboceanu
Director: Oriol Gomis Bellmunt
Codirector: Eduardo Prieto Araujo

Handed in: June 2017

Escola Tècnica Superior
d'Enginyeria Industrial de Barcelona

Review

Coming as an answer for the high demand of renewable energy (especially at distribution level) and seeing the benefits of Direct Current (DC) microgrid concept (both technical and economical) that enables the integration of renewable sources, this thesis proposes a voltage droop control strategy for a generic grid connected DC microgrid to ensure stability and performance of the system.

DC microgrids can have different configurations with different renewable sources that affect the system in a certain way. In this thesis only solar generation is considered using a simplified model. Since it desired to design this control strategy so that is applicable to any microgrid configuration (with minor changes), a generic multiterminal configuration has been analyzed. All components of this configuration are interconnected through power electronic converters. Focusing on the DC side of the microgrid, these converters are responsible for maintaining the grid voltage under reasonable limits. For this purpose, a power based droop control solution is proposed to control the DC voltage fast, as well as to establish power sharing between converters connected to the DC grid.

All grid elements affect the droop performance in a certain way. In order to perform a proper design, a complete dynamic analysis is described, by creating a detailed linear model of the entire system. Based on this linear model, certain control techniques are applied to determine the best droop constants to ensure that the performance specifications are met (keep the voltage within the limits and avoid over currents in converters)

This droop design is validated through simulations in Matlab/Simulink, where a three terminal microgrid is analyzed (a PV plant is connected to the AC grid through two identical voltage source converters). Linear and non linear models show identical dynamics. The droop controller responds adequately to the changes caused by the intermittent nature of solar radiation, and keeps the voltage within the limits, which confirms that the linear model is suitable for droop design.

The droop design shows an adequate response of the system. This design can be applied to any multiterminal configuration with some changes in the linear model and the tuning process. This methodology is also validated through a paper for the 2017 International Conference on DC Microgrids (ICDCM)

Contents

List of Abreviations

PV	Photovoltaic
DC	Direct Current
AC	Alternating Current
EMI	Electromagnetic Interference
DG	Distributed Generation
MPPT	Maximum Power Point Tracking
IGBT	Insulated-Gate Bipolar Transistor
VSC	Voltage Soure Converter
LCC	Line Commutated Converters
RC	Resistor-Capacitor
SOC	State Of Charge
PWM	Pulse Width Modulation
ACG	Automatic Generation Control
L-C	Local Controller
MGCC	Microgrid Central Controller
MIMO	Multiple Input Multiple Output
LTI	Linear Time Invariant
LC	Rezonant Circuit
PCC	Point of Common Coupling
PLL	Phased Locked Loop
PI	Proportional Integral
IMC	Internal Model Control
SVD	Singular Value Decomposition
SISO	Single Input Single Output
TSO	Transmission System Operator
IRR	Internal Rate of Return

1. Preface

1.1 Context

Renewable energy is one of the most popular topics of current days, debated at a global level by many administrations, companies and institutions. This transition to the so called "clean energy" is not only necessary for the planet's ecological survival; it's critical to the health and well being of every person [1]. It has a huge implication in every aspect of todays society: social, economical, political, environmental etc. Issues like global warming, climate change, high oil prices triggered a large interest in this field, in the last years. Many countries have taken action towards this mitigation. For example European Union has set a directive to achieve 20 % renewable generation by the year of 2020. This rapid deployment in renewable sources, with many benefits, rises some technical challenges.

One challenge (which is of interest in this thesis) is incorporating these renewable sources in the distribution system with high efficiency, minimal costs, and keeping the system stable. Before connecting a significant amount of renewables to the power grid, the existing network must suffer some changes in order to:

- allow a bi-directional power flow, meaning the end user will be able to contribute to the electricity supply. This is to ensure stability in the grid when adding more distributed sources;
- have a grid management system who's purpose is to reduce peak loads, making the grid more flexible and ensuring security of supply;
- improve interconnection of grids on all levels for more reliability and stability;
- introduce mechanisms that ensure stability and control of the grid (power balance, frequency, voltage) to cope with the intermittent nature of renewable sources;

Smart grid concept can be applied to enable these changes, by combining grid elements of smart functionality with communication and information technologies for a better efficiency, reliability, flexibility, along with other benefits. By means of power electronics (key component in smart grid technology) future renewable plants will be able to participate in the frequency control by regulating the active power flow (with proper algorithms) and control the voltage, fault ride-through capability and reduce losses through reactive power control [2].

1.2 Origin of the project

At residential and/or commercial level, photovoltaic panels (PV) are considered the most obvious and suitable choice when it comes to green electricity [3]. Running costs are low, they fit well from an aesthetic point of view, but they do not generate electricity during night time.

From this viewpoint we will have a PV integration walk through, from the power plant itself to the local consumer. PV modules produce DC power. This power needs to be converted to AC and also synchronized with the commercial grid frequency, to reach the end user. To reduce power losses over the transmission network, the voltage level needs to be increased. Before it reaches the residential outlet, the power is changed to a lower voltage level, through a series of substations and transformers. So an efficient transmission and distribution system needs to be considered related to cost, lifetime, and intermittent nature of solar radiation.

DC microgrids become a more and more interesting idea whose purpose, among many others, is to minimize or eliminate these conversions that causes a high proportion of losses. According to [4] DC microgrids reduces these conversion losses from 32% to 10%. Lots of research has been done for DC microgrids as an integration tool for renewable sources. Technical and economical benefits become more and more evident but they also raise a series of challenges. One of the challenges, that is addressed in this thesis, is assuring voltage stability in the system when these solar plants are connected to the grid through a DC microgrid

1.3 Benefits and challenges of DC microgrids

Apart from integrating more renewables, DC microgrid concept has many other advantages and applications. For example, different DC microgrid architectures can facilitate the design of ultra-available power sources for critical loads, such as hospitals, security units, data centers etc [5]. Statistically it has been proven that, for critical loads, DC systems have a higher availability over AC systems (at least two orders magnitude higher) [6]. On top of that DC facilitates integrating majority of modern electronics since all of them internally work on DC supply.

Coming back to renewable sources, a few advantages are worth mentioning when using DC microgrid technology:

- Reduced power losses in the system by reducing the number of AC/DC conversions;
- Loads can be supplied with energy through the distribution line when there is a blackout in the commercial grid; but to have high local availability it is important to have different power sources in reduntant architectures, or to have local storage [5];
- There is no need to synchronize distributed generators;
- Fluctuations of generated power and also of the loads can be compensated through energy storage modules;
- The system does not require long transmission lines, or high capacity lines;

Among so many benefits, this concept rises a couple of difficulties. As mentioned before DC systems do not experience harmonic issues because the fundamental frequency of a DC system is 0 Hz and integral of multiple frequencies of 0 Hz other than the fundamental does not exist. But in reality voltage oscillations could come from grid resonances, controller interactions so, the discussion of harmonics to DC system is relevant. In microgrids multiple power electronic converters

are connected to a DC bus and nonlinear effects of these converters can cause oscillations, damaging resonance or unacceptable electromagnetic interferences (EMI). Special filters must be designed to mitigate these "harmonic" currents.

Another issue that needs to be addressed in microgrids is the impact of fault currents. In DC systems fault currents can be drawn only through converters, so the current is limited by the power rating of these converters. Low available fault current in the system can create voltage disturbances in other points and also makes difficult to select the proper protection settings that will accurately differentiate between fault current and heavy load condition.[7] In addition the DC distribution system will also suffer from absence of periodic 0 crossings. This is especially problematic for arc faults.

Grounding is another problem that needs attention and is closely related with the fault issue discussed earlier. The grounding configuration has an impact on power quality and safety of the system in fault conditions.

1.4 Motivation of the project

Microgrids have some challenges that need to be dealt with. One of them is the intermittent nature of solar radiation which causes serious issues in voltage stability. In this thesis, the focus more in the control part of the microgrid to ensure stability in the system. More specifically, a control strategy based on voltage droop control that takes into account all grid dynamics is proposed. There are some other droop strategies presented in the literature such as current based droop controllers. Here it is suggested a power based droop control for a certain microgrid system that aims to reduce voltage fluctuations caused by the varying output of the solar panels. This will ensure not only the the grid stability keeping certain variables withing their limits but also can reduce converter power ratings, with potential economical benefits.

2. Introduction

2.1 Scope

Renewable sources have increased in popularity in last years for a number of reasons as described above. So the newest trend is to reduce dependency on conventional power plants (with a finite resource) that have a huge impact on the environment and to rely more on renewable sources. Even though the current infrastructure and legislation in many countries does not allow to inject power produced by renewables installed at household level, this will change slowly change in the future as technical and economical benefits of microgrid concept become more and more evident.

This thesis aims to provide a adequate control strategy, based on droop voltage control, of a generic multiterminal DC microgrid to facilitate integration of renewable energy at distribution level, assuring grid stability, efficiency and a certain performance level. This strategy is thought so it can be applied to different microgrid configurations with minor changes.

2.2 Objectives

Microgrids can have different configurations and can be composed of grids of different nature forming hybrid AC/DC systems interconnected through power electronic converters. On the DC side, these converters are in charge of maintaining to voltage within certain levels and limits. For this purpose, a droop control strategy is proposed to assure a fast DC voltage regulation.

To see how different elements of the DC grid affect the droop performance, a complete dynamic analysis of the DC microgrid system is required. This is done by performing a detailed study on the linearized model of the system. Based on this linear model different control design techniques will be applied to on the droop controller. Then this theoretical design is validated through a multiterminal DC microgrid in Matlab/Simulink to test the performance.

3. DC Microgrid

3.1 General Overview

The need for flexible and reliable power systems with communication and control systems has led to the creation of the smart grid concept [8]. Future modern grids will need to deal with increasing distributed sources (especially renewables sources with intermittent nature) assuring an optimum performance during and after certain events (faults, generation/load changes etc.)

A hybrid AC/DC microgrid (element of the smart grid concept) is presented in Figure 3.1. It has two main parts, the AC side and the DC side. The AC part consists of the main AC grid (medium or low voltage) among with AC conventional loads. The DC side contains all distributed generation (DG) points, charging stations for electrical vehicles (EVs) and storage modules, all connected via DC/DC converters, due to their DC nature.

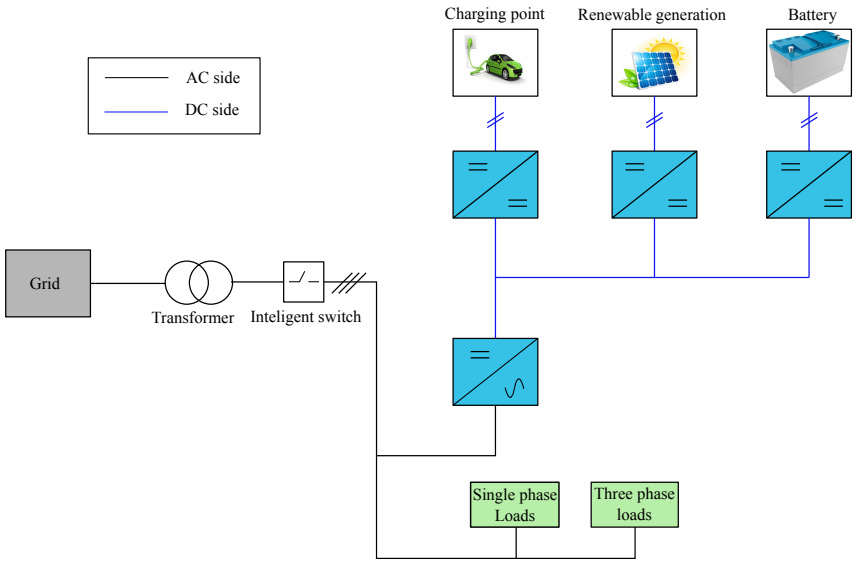

Figure 3.1: Hybrid AC/DC microgrid

Power electronics is a key technology in transforming the traditional power systems into smart grids because they allow a fast power flow and voltage control (in range of milliseconds). AC/DC converters are key elements in grid connected microgrids as they synchronize the delivered power from the microgrid with the grid frequency and require a bidirectional power flow. Active and reactive power control is required to assure power balance and voltage stability.

Solar converters are DC/DC converters that inject generated power in the grid and they are configured to maximizes the output solar energy by performing Maximum Power Point Tracking (MPPT).

Storage modules based on batteries also requires bidirectional DC/DC converters either to inject power in the grid or to charge the battery.

DC cable connects all parts belonging to DC current. Usually it has a resistance

in its line. Comparing AC cable with DC cable, a few advantages can be noticed. DC cables transfer electricity more efficiently and with less conductor material compared to AC cables. Hence they offer both cost reduction and sustainability features [9],[10].

A big variety of converter topologies can be used [8] to connect the microgrid to the main grid. The most common ones are Insulated-Gate Bipolar Transistor (IGBT) based inverters, also called as Voltage Source Converters (VSC). They operate at high switching frequencies and can control independently active and reactive power.They also reduce the injected harmonic content implying smaller filters. But these high frequencies also imply high losses, one of the main disadvantage of this technology.

Inverters can be classified based on levels number. Two level converter is the most common type in low voltage applications. For high voltages a multilevel configuration can be used, such as H-bridge converters or flying capacitors. [8]

Another significant requirement for microgrids and connecting renewable sources (especially wind farms) is the voltage ride-through capability. This means that the concerned system cannot disconnect whenever a fault occurs. This is most important for nodes where large power is injected in the grid, enough to produce instability in the main grid.

The following sections describe working principles and models of all microgrid components, related to the simplified structure described in Figure 3.1.

3.2 Photovoltaic plant

For domestic power level, renewable energy based on photovoltaic modules is one of the most popular and suitable solution, also supported by certain governments in Europe through increasing incentives. It is important derive a proper model of the PV plant for cost and performance evaluation. However these models will never match real PV modules provided by a certain manufacturers because certain variables like short circuit current or the open circuit voltage will change as the modules get older [11].

PV generation is dependent of certain variables, as described in Figure 3.2.

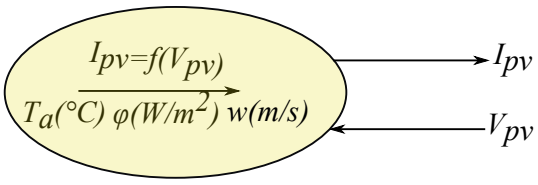

Figure 3.2: PV parameters [12]

The model inputs are the solar irradiation ϕ, the ambient temperature T, the wind speed w and the photovoltaic generator voltage V_{pv}, whereas the output is the current which is supplied by the panel [12].

Another simple model proposed in [13] is described in Fig.3.3. This is the simplified one-diode model that uses only four parameters. But this model doesn't take into account solar irradiation which may cause some voltage errors in the I-V curve.

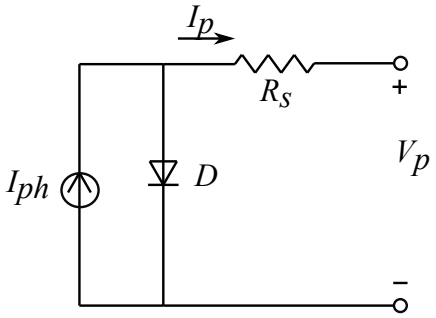

Figure 3.3: Simplified PV model

A more complete model which takes into account parameters provided by manufacturers is described in [12]. One of the advantages of this model is that it doesn't require any numerical method.

The output current of a PV model, as a function of voltage can be written as:

$$I_p = I_{SC}[1 - C_1(e^{(\frac{V_F}{C_2 V_{OC}})} - 1)] \tag{3.1}$$

C_2 and C_1 are coefficients that can be expressed as:

$$C_1 = (1 - \frac{I_{MPP}}{I_{SC}})(e^{(\frac{-V_{MPP}}{C_2 V_{OC}})}) \tag{3.2}$$

$$C_2 = \frac{(\frac{V_{MPP}}{V_{OC}} - 1)}{\ln(1 - \frac{I_{MPP}}{I_{SC}})} \tag{3.3}$$

where I_{SC} is the short circuit power, V_{OC} is the open circuit voltage, V_{MPP} is the maximum power point voltage and I_{MPP} is the maximum power point current. These parameters can be expressed as follows:

$$I_{SC}(G,T) = I_{SCS}\frac{G}{G_S}[1 + \alpha(T - T_S)] \tag{3.4}$$

$$V_{OC}(T) = V_{OCS} + \beta(T - T_S) \tag{3.5}$$

$$I_{MPP}(G,T) = I_{MPPS}\frac{G}{G_S}[1 + \alpha(T - T_S)] \tag{3.6}$$

$$V_{MPP}(T) = V_{MPPS} + \beta(T - T_S) \tag{3.7}$$

I_{SCS}, V_{OCS}, I_{MPPS} and V_{MPPS} are parameters defined at standard conditions ($G_S = 1000W/m^2$) and α and β are current and voltage temperature coefficients. These parameters described above are usually provided by the manufacturers in the data sheet.

3.3 Storage based on batteries

Storage units, usually based on batteries, are key components in DC microgrids. They are important to flatten the demand curve and also for the functionality of the microgrid in islandic mode. To adapt to short term power surplus or shortage, the

storage must charge and discharge very frequently under varying current conditions [14].

There are multiple categories of battery models, depends on the application: electrochemical models, mathematical models or electrical models. The electrochemical model is mainly used for design aspects of the batteries and relate design parameters with macroscopic (voltage and current) and microscopic (concentration distribution) information. Mathematical models are usually too abstract to implement in practical applications. They are useful in mathematical approaches to predict the battery behavior, efficiency, capacity or battery runtime. But they cannot offer any I-V information which is necessary for circuit simulation and optimization applications. Electrical models are most useful and intuitive for electrical engineers because they use a combination of electrical components such as voltage sources, resistors and capacitors, making them easy to implements circuit simulators.Most of electrical models can be classified in three categories: Thevenin model, impedance model and runtime model [15].

The most basic form of the Thevenin-based model is described in the figure bellow:

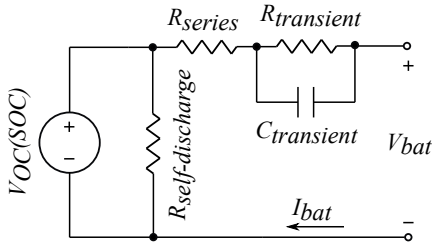

Figure 3.4: Thevenin battery model

This model uses a resistor R_{series} and an RC parallel ($R_{transient}$ and $C_{transient}$) to anticipate the battery response to transient loads at a certain state of charge (SOC), by assuming that the open circuit voltage $V_{OC}(SOC)$ is constant. One of the drawbacks of this model is that it cannot accurately predict battery runtime in circuit simulations [15].

The impedance battery model, as described in Figure 3.5, is based on electrochemical impedance spectroscopy to obtain an AC-equivalent impedance model, and then use a network equivalent (Z_{AC}) to fit the impedance spectra. The fitting part is a very difficult and complex process. As well as the Thevenin model it cannot predict the battery runtime [15].

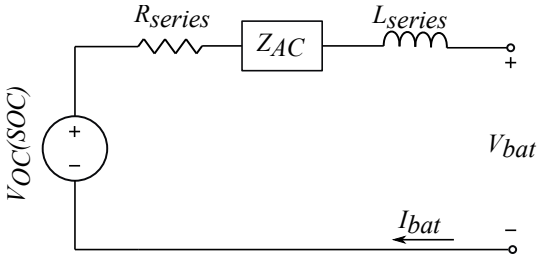

Figure 3.5: Impedance battery model

The runtime models, as described in Figure 3.6 is a very complex model that simulates battery run time and DC voltage response for a constant discharge current.

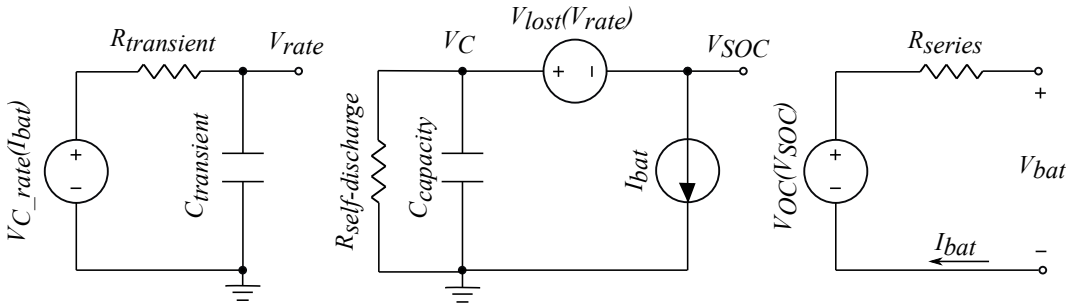

Figure 3.6: Runtime based battery models

Non of these models described above can predict both battery runtime and I-V performance accurately and in the same time. Therefore, a combination of these three models is desired for system integration and optimization [15].

3.4 Voltage Source Converter(VSC)

3.4.1 VSC structure

Majority of DC microgrids are connected to the grid for a safer and continuous operation through a grid converter. Voltage source converters (VSC) are a very popular solution to transfer power between AC and DC sides. A generic system with a grid connected VSC is presented in Figure3.7. The converter is made of the

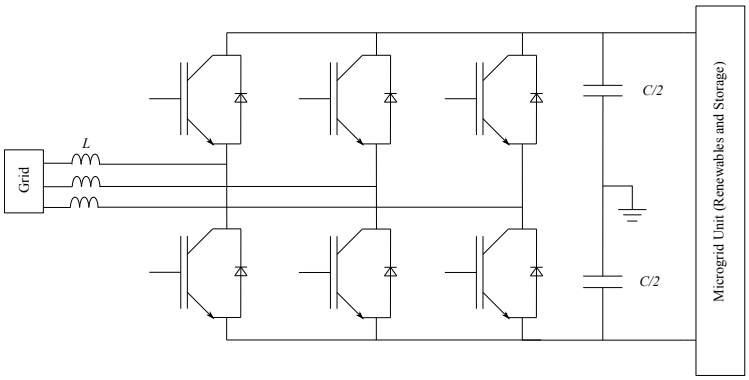

Figure 3.7: Grid connected VSC

bridge itself, reactor, the DC capacitor and the AC filter. It is a six pulse bridge converter with two levels and series IGBTs in each valve. Every IGBT has an antiparallel diode [16]. The inductance allows a smooth connection of the converter to the grid. The DC capacitor acts as an energy storage to control the power flow and to provide a low inductive path for turned-off currents. It also reduces harmonic content on the DC side.

The converter controller calculates the necessary voltage time area across the reactor to change the reactor current from the present value to the nominal one. Current order to the controller is calculated either based on a set power/current order or based on the DC voltage control. A reference voltage with the same amplitude and

frequency with the the fundamental output of the bridge, is calculated. Then the switch control signal in the IGBTs (which controls the on or off state of the switch) is generated by pulse width modulation (PWM) where the sinusoidal reference voltage is compared with a triangular waveform. When the reference voltage is higher than the tiangular signal the phase terminal is connected to the positive DC terminal and if it is lower than it is connected to the negative terminal [16].

The microgrid unit is connected on the DC side of the converter. It can contain photovoltaic pannels or batteries which have a DC nature but they're often connected through inverters to adjust the voltage level. Regarding wind farms, they produce power of varying frequency so it is converted into DC before it is injected in the grid. Overall, the DC side can be modeled as either a DC voltage source or as a current source in parallel with a capacitor. The AC side is usually modeled by utility grid Thevenin equivalent or in an even more simplified way as AC voltage source [8].

3.4.2 VSC modeling

Even though the converter functions based on the switching state of IGBTs, for control purposes (which is the main focus of the thesis) it is more convenient to use a simplified model. This model relies on separating the AC and the DC side, as shown in the Figure 3.8. The AC side is modeled as a three phase voltage source

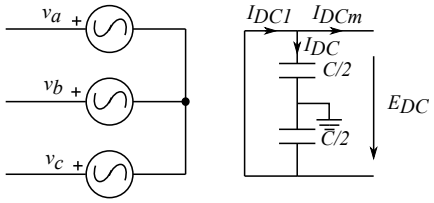

Figure 3.8: Grid connected VSC [8]

whereas the DC side is modeled as a current source in parallel with capacitor. The two sides are connected through a power equation that neglects converter losses.

$$I_{DC1} = \frac{P_{ac}}{E_{DC}} \tag{3.8}$$

where I_{DC1} is the DC current of the current source, P_{ac} is the active exchanged with the AC grid, and E_{DC} is the DC bus voltage.

The DC side capacitor is obtained from the following equation:

$$I_{DC} = C\frac{dE_{DC}}{dt}, \quad I_{DC1} - I_{DCm} = C\frac{dE_{DC}}{dt} \tag{3.9}$$

Integrating the expression above, the DC voltage as a function of current is:

$$E_{DC} = E_{DC0} + \frac{1}{C}\int_0^t I_{DC}dt = E_{DC0} + \frac{1}{C}\int_0^t (I_{DC1} - I_{DCm})dt \tag{3.10}$$

3.4.3 Voltage equations in the synchronus reference frame

The ac side of the converter can modeled as in Figure 3.9.

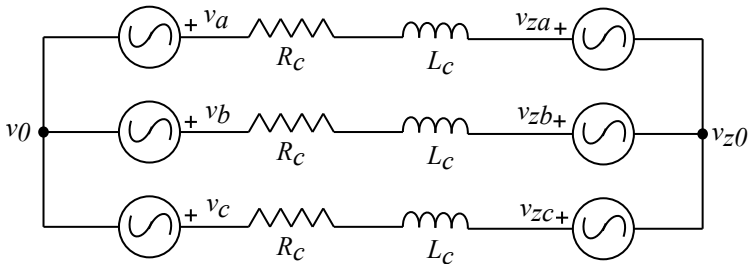

Figure 3.9: AC side representation of the grid converter (VSC) [8]

Based on this model the voltage equation is:

$$\begin{bmatrix} v_{za} \\ v_{zb} \\ v_{zc} \end{bmatrix} - \begin{bmatrix} v_a \\ v_b \\ v_c \end{bmatrix} - (v_0 - v_{z0}) \begin{bmatrix} 1 \\ 1 \\ 1 \end{bmatrix} = \begin{bmatrix} r_c & 0 & 0 \\ 0 & r_c & 0 \\ 0 & 0 & r_c \end{bmatrix} \begin{bmatrix} i_a \\ i_b \\ i_c \end{bmatrix} + \begin{bmatrix} l_c & 0 & 0 \\ 0 & l_c & 0 \\ 0 & 0 & l_c \end{bmatrix} \frac{d}{dt} \begin{bmatrix} i_a \\ i_b \\ i_c \end{bmatrix} \tag{3.11}$$

where v_a, v_b and v_c are grid voltages in the *abc* frame, v_{za}, v_{zb} and v_{zc} are converter instantaneous voltages in the *abc* reference frame, i_{abc} are three phase currents in *abc* reference frame, r_c and l_c are equivalent resistance and inductance. v_0 and u_0 are voltages at the grids neutral and at the converter. If there is no neutral conductor the difference between them is 0. Considering this and applying Park transformation to the previous equation we get:

$$\begin{bmatrix} u_q \\ u_d \end{bmatrix} - \begin{bmatrix} v_q \\ v_d \end{bmatrix} = \begin{bmatrix} r_c & l_c\omega_e \\ -l_c\omega_e & r_c \end{bmatrix} \begin{bmatrix} i_q \\ i_d \end{bmatrix} + \begin{bmatrix} l_c & 0 \\ 0 & l_c \end{bmatrix} \frac{d}{dt} \begin{bmatrix} i_q \\ i_d \end{bmatrix} \tag{3.12}$$

where the *qd* index stands for *qd* reference frame and ω_e is the electrical angular velocity [8].

3.5 DC-DC converters

Even though most of renewable sources and storage units have a DC output they need to be connected to the microgrid through DC-DC converters.

For example PV panels are connected through a boost converter to raise the output voltage level at the nominal microgrid level and to track the maximum power point of the solar output which fluctuates depending on the solar irradiation. The most basic model of the boost converter is described in Figure 3.10. Based on the

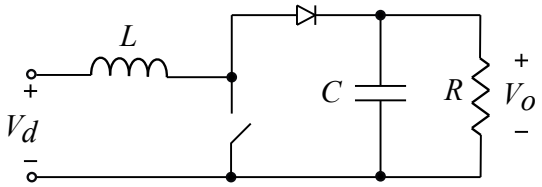

Figure 3.10: Step-up DC-DC converter [17]

state of the switch the voltage equation can be written as:

$$V_d t_{on} + (V_d - V_o) t_{off} = 0 \tag{3.13}$$

where V_d is the input voltage, V_o is the output voltage, t_{on} is the duration the switch is ON and t_{off} is the duration the switch is OFF. By dividing both sides of the converter with the switching period T_s we obtain:

$$\frac{V_o}{V_d} = \frac{T_s}{t_{off}} = \frac{1}{1-D} \tag{3.14}$$

where D is the duty ratio. If we assume that the converter doesn't have any losses:

$$V_d I_d = V_o I_o \tag{3.15}$$

and

$$\frac{I_o}{I_d} = (1-D) \tag{3.16}$$

Storage units based on batteries require a bidirectional DC-DC converter, to provide power when other sources are not present and to accumulate energy when the storage system is not needed.The characteristics of the converter should look like in Figure 3.11.

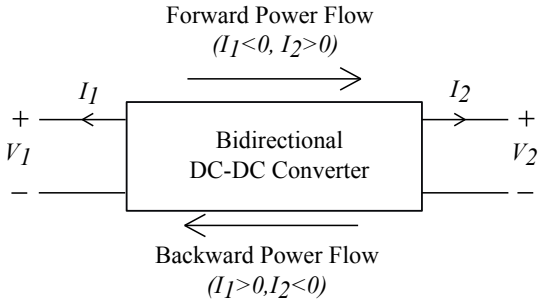

Figure 3.11: Bidirectional converter characteristics

One of the most popular converter used in batteries is the half bridge dc-dc converter. A simple schematic of this converter is presented in Figure3.12.

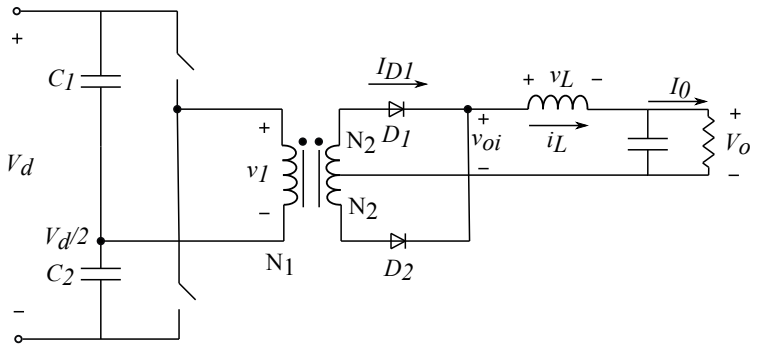

Figure 3.12: Half bridge DC-DC converter model [17]

The relation between the input voltage and the output voltage for the half bridge converter is described by the following equation:

$$\frac{V_o}{V_d} = \frac{N_2}{N_1} D \tag{3.17}$$

3.6 DC cable

All distributed sources in the microgrid are connected to the grid (through voltage source converter). DC capacitors have a strong impact on the voltage so the first model is just a resistor-capacitor (RC) model depicted in Figure 3.13.

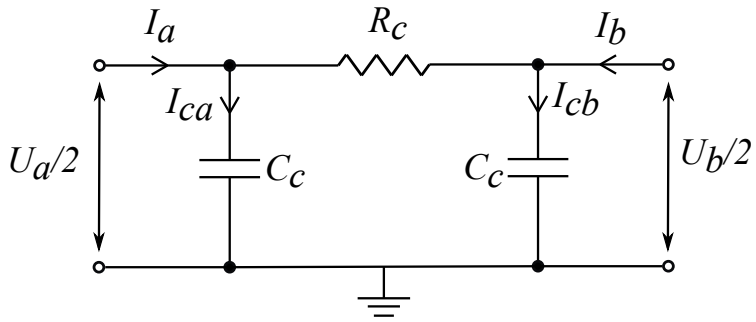

Figure 3.13: RC cable model [18]

Another cable model, which is more popular in simulation environments is the classical PI model described in Figure 3.14.

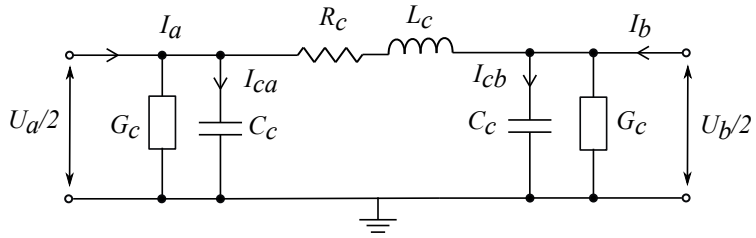

Figure 3.14: PI cable model [18]

4. Control Structure

4.1 AC and DC network similarities

All electric power systems must have, at any moment, between electric energy generation and consumption. To maintain this balance, automatic control systems are required that can respond very fast (in matter of seconds). In AC systems this is done by Automatic Generation Control (ACG), which is a hierarchical strategy, as seen in Figure 4.1.

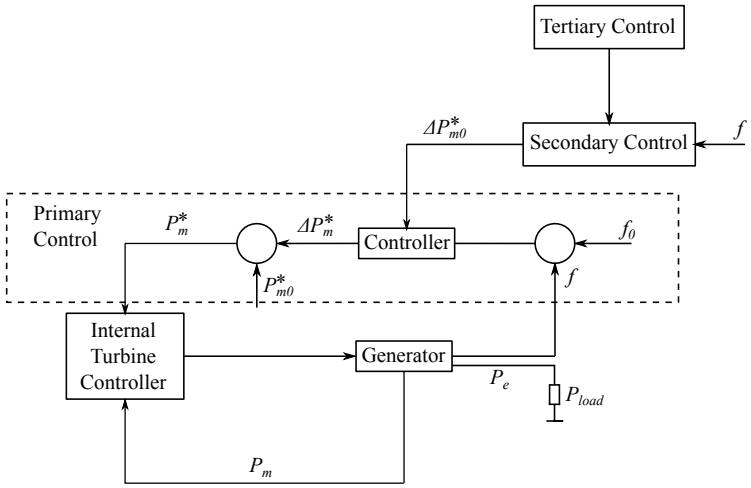

Figure 4.1: Conceptual AC hierarchical control scheme

Primary control is designed to adjust sudden load/generation changes. A load decrease and/or a generation increase causes frequency changes. Each synchronous system has a separate primary control. Power plants participating in this regulation have an internal controller that constantly checks the ratio between frequency deviation (Δf) and power reference change (ΔP^*_{mec}), also named proportional gain. The generator has an internal inertia that supplies the difference between electrical power and mechanical power, until the primary control changes the mechanical power accordingly. Frequency dynamics can be characterized by this linear equation, as proven in [19]:

$$\Delta f = \frac{f_0}{2H_{ac}S_B}\left(\Delta P_{mec} - \Delta P_e\right) \tag{4.1}$$

where S_B is the nominal power of the machine and H_{ac} is the inertial constant.

After the imbalance is eliminated by the primary control, the frequency will deviate from the nominal value. On top of that systems reserve will partly be used up, so it will be difficult to respond to new imbalances. This is where the secondary control steps in. Its main functions are [20]:

- restore frequency to its nominal value (50 Hz in Europe or 60 Hz in North America);

- release used primary control reserves, so that the system can deal with new load/generation changes;
- prevent the time deviation from increasing;

Tertiary control is an automatic or manual system that changes the working points of participating units, to restore an adequate secondary control reserve.

It is important to note that frequency dynamics in the generators are very similar with DC voltage dynamics in the power converter output. Using the ACG system described earlier, an analogy can be created as seen in Figure 4.2. The generator

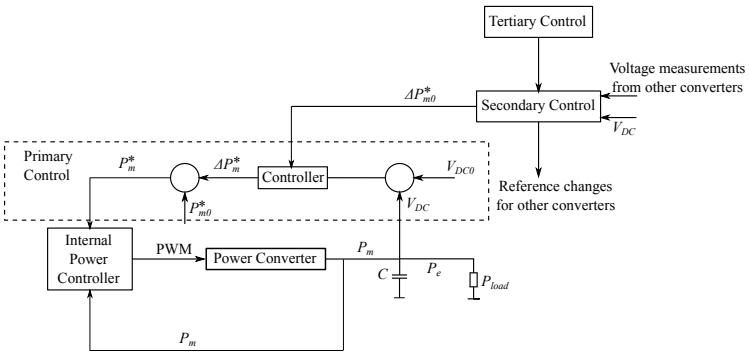

Figure 4.2: Conceptual DC hierarchical control scheme

is switched with a power converter and the internal inertia becomes the DC bus capacitor (C). Similarly, the voltage DC dynamics can be described by the following equation, as demonstrated in [19]

$$\Delta V_{DC} = \frac{V_{DC0}}{2H_{dc}S_B}\left(\Delta P_{mec} - \Delta P_e\right) \tag{4.2}$$

For the sake of analogy the P_{mec} and P_e were maintained and the represent the power flowing in and out of the DC capacitor. In this equation, the term H_{dc} can be called inertial constant of the dc bus capacitor (it doesn't represent the same concept as H_{ac}) . This term represents the ratio between stored energy in the capacitor at nominal voltage and the rated power of the converter S_b.

Considering the similarities between the two dynamics, as it can be seen in the equations (4.1) and (4.2), at a first glimpse it seems normal to apply the same control strategy. However there are some differences between the two systems that make this idea a bit problematic.

First of all, AC voltages are characterized by three parameters: amplitude, frequency and phase. Voltage magnitude is directly related to reactive power, while frequency and phase are directly related to active power.

In DC systems, voltages are characterized by only one parameter, the amplitude. There is no reactive power and both the power flow and the power imbalance are reflected into the voltage magnitude, so its difficult to apply the same strategy [19].

4.2 DC microgrid control challenge

A generic multiterminal DC microgrid scheme can be seen in Figure 3.5. This system is built to connect multiple generation plants in the distribution grid. All converters are interconnected in the DC side of the grid.

Solar converters are DC/DC converters that inject generated power in the grid and they are configured to maximizes the output solar energy by performing Maximum Power Point Tracking (MPPT).

Grid side converters, apart from transforming the generated power into AC power and synchronize it with the grid, also control the DC voltage.

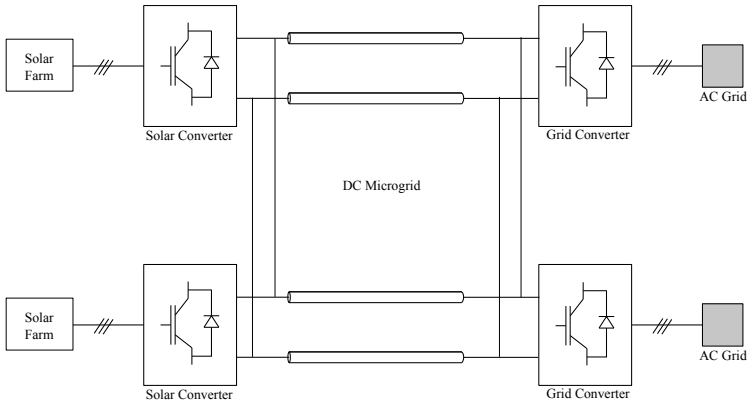

Figure 4.3: Multiterminal DC microgrid [21]

The multiterminal DC microgrid poses multiple challenges because connected elements continue to change in terms of power and voltage level. Different converters are interfacing the DC microgrid with the AC system. This makes controlling DC voltage quite difficult. Different control strategies can be applied, either using a single or several converters to maintain the voltage in the desired limits. Using a single converter is a simple solution because only that one controls the DC voltage in the system whereas the others operate in power regulation mode. This method presents some drawbacks, such as power sharing among converters or loss of the main converter due to an outage that would create a grid failure.

4.3 Other control strategies

There are multiple control strategies proposed in the literature to deal with all these issues. In [22] hierarchical control architecture is depicted, where the author focuses on primary and secondary control of a DC microgrid. Each converter connected to the grid has a local controller or LC (primary control) which is coordinated and supervised by a microgrid central controller or MGCC (secondary control). AC-DC converters are controlled using a vector decouple technique, whereas DC-DC converters (associated with the distributed generation) is controlled using a tracking maximum power point algorithm.

The author in [23] presents a fuzzy control strategy combined with dynamic programing for a small type islanded DC microgrid, to keep the power balance between generation and load and keep the voltage stable. The design for the Fuzzy Logic Controller has multiple stages which can be resumed in a Multiple Input Multiple Output (MIMO) control system.

In [24] it is presented an agent-based distributed hierarchical control strategy of DC microgrid systems. This architecture consists of primary current sharing control based on an adaptive virtual resistance, secondary voltage restoration control and tertiary agent for global information discovery and optimization.

This thesis proposes a control strategy for a multiterminal DC microgrid with multiple renewable sources and to observe the system behavior. The control system is designed taking into account the complete dynamics of the multiterminal grid, including linearized dynamics of the AC and DC grid and the converter controllers [8].

4.4 Proposed control strategy - droop voltage control

The alternative solution would be to regulate the DC grid voltage employing distributed droop control using several converters. This method is applied locally at each converter, so there is no need for communication between them. Absence of the communication link improves reliability without adding any constraint regarding physical location of the module. Also this method allows power sharing between converters acting over the power loop as it can be seen in Figure 3.6. Any deviation in power sharing can be compensated using upper level controllers that operate in a slower time frame. A complete droop control scheme is presented in Figure 3.6. The upper control system will not be considered in this analysis; this thesis will focus on the droop design considering the overall grid dynamic behavior [21],[25].

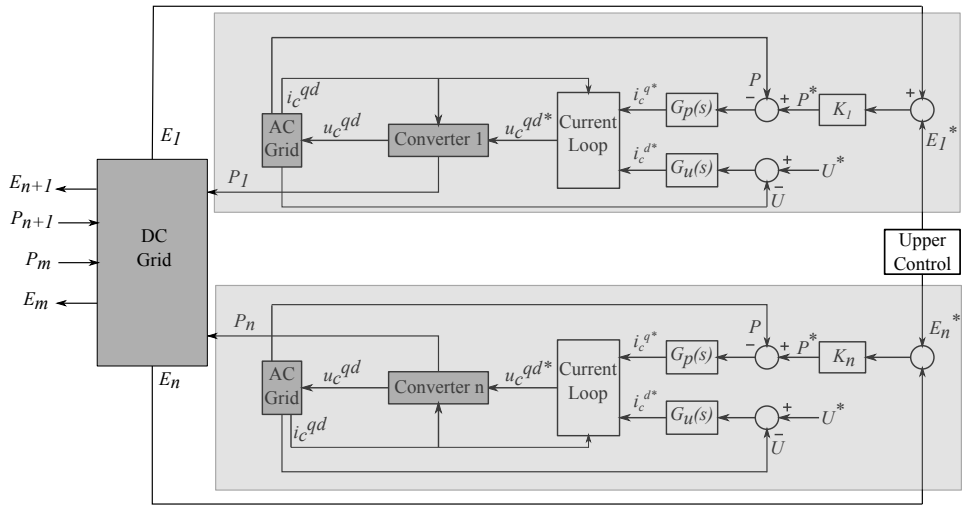

Figure 4.4: Complete microgrid control scheme

There are multiple types of droop control presented in the literature. Here the it will be presented the power-based droop control method. For n converters the law can be expressed as:

$$P^* = K(E - E^*) \tag{4.3}$$

where E is the the voltage measured at the DC terminals of the converter, E^* is the reference voltage for the droop controller (it can be different for each converter), K is the droop constant an P^* that goes in the power loop (as seen in Fig.3.6). This power controller (G_p) regulates the power going through the converter to track the DC grid voltage reference, also considering a DC voltage error caused by the proportional nature of the droop controller. AC voltage is controlled by the voltage regulator G_u. The outputs of the power and AC voltage regulators go in the inner current loop, that applies voltages in the AC grid.

Dynamics of interconnected systems can affect voltage regulation. So, to perform a proper control, different dynamics must be considered, such as DC grid dynamics, AC grid dynamics, converters and filters dynamics [21].

5. System Linear Modeling

As mentioned before, for a proper control design that includes system dynamics, linear model of the entire grid must be derived. This chapter will present some basic elements of linear system theory and will derive linear model of the system that will be used in the controllers design procedure.

5.1 State-space reprezentation

Let us consider a general system, whose inputs are represented by vector u (of order $m \times 1$) and the outputs represented by vector y (of order $l \times 1$). This system is described by the state vector x (of order $n \times 1$). The non-linear state space model is described by:

$$\dot{x} = f(x,u); \quad y = g(x,u) \tag{5.1}$$

where $\dot{x} = \frac{dx}{dt}$ and f and g are nonlinear functions. After linearization, the linear state-space model of the above system looks like:

$$\dot{x} = Ax(t) + Bu(t) \tag{5.2}$$

$$y(t) = Cx(t) + Du(t) \tag{5.3}$$

where:

- A is the state matrix of order $n \times n$;
- B is the input matrix of order $n \times m$;
- C is the output matrix of order $l \times n$;
- D is a matrix of order $l \times m$;

Usually the dependence of time for x, y, u is neglected to simplify things. Then the system becomes linear-time invariant (LTI):

$$\dot{x} = Ax + Bu \tag{5.4}$$

$$y = Cx + Du \tag{5.5}$$

These equations describe the dynamic behaviour of a rational, linear system. This system can be rewritten in a matrix form as:

$$\begin{bmatrix} \dot{x} \\ y \end{bmatrix} = \begin{bmatrix} A & B \\ C & D \end{bmatrix} \begin{bmatrix} x \\ u \end{bmatrix} \tag{5.6}$$

In equations (5.2) and (5.3) u represents all independent variables. Usually there are three kind of independent variables: manipulated inputs u, disturbances d and measurement noise n (but it is disregarded in this thesis). For a more complex analysis these variables must be considered and the LTI state space must be updated [26].

5.2 AC Grid Modeling

In this section, the converters grid connection will be further analyzed and a linear model will be derived. The converter is connected to the grid through an inductance and capacitance filter (LC) as it can be seen in Figure 5.1 [21].

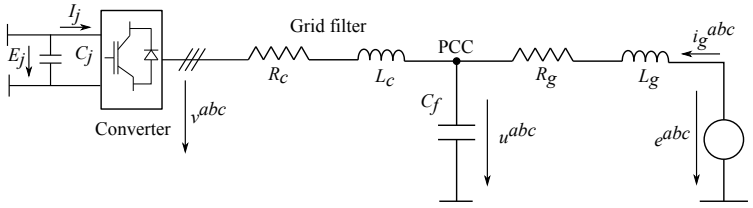

Figure 5.1: VSC connected to the grid

The grid is modeled as a simple Thevenin equivalent. Including the LC filter in the model, the state-space representation of the converter is:

$$\frac{dx_{lc}}{dt} = A_{lc}x_{lc} + B_{lc}u_{lc} \tag{5.7}$$

where A_{lc} and B_{lc} are:

$$A_{lc} = \begin{bmatrix} -\frac{R_c}{L_c} & -\omega & \frac{1}{L_c} & 0 & 0 & 0 \\ \omega & -\frac{R_c}{L_c} & 0 & \frac{1}{L_c} & 0 & 0 \\ -\frac{1}{C_f} & 0 & 0 & -\omega & \frac{1}{C_f} & 0 \\ 0 & -\frac{1}{C_f} & \omega & 0 & 0 & \frac{1}{C_f} \\ 0 & 0 & -\frac{1}{L_g} & 0 & -\frac{R_g}{L_g} & -\omega \\ 0 & 0 & 0 & -\frac{1}{L_g} & \omega & -\frac{R_g}{L_g} \end{bmatrix} \tag{5.8}$$

$$B_{lc} = \begin{bmatrix} -\frac{1}{L_c} & 0 & 0 & 0 \\ 0 & -\frac{1}{L_c} & 0 & 0 \\ 0 & 0 & 0 & 0 \\ 0 & 0 & 0 & 0 \\ 0 & 0 & \frac{1}{L_g} & 0 \\ 0 & 0 & 0 & \frac{1}{L_g} \end{bmatrix} \tag{5.9}$$

L_c is the converters filter inductance, R_c is the parasitic inductance, ω is the grid's frequency ($\omega = 2\pi f$) and L_g and R_g are inductance and resistance from the grid Thevenin equivalent. For the LTI system described in equation 5.7 the state vector will be:

$$x_{lc} = (i_c^q, i_c^d, u^q, u^d, i_g^q, i_g^d) \tag{5.10}$$

where i_g^{qd} are the currents flowing from the point of common coupling (PCC) to the converter, i_g^{qd} are currents flowing from the grid and u^{qd} are voltages at the PCC. The input vector will be:

$$u_{lc} = (v^q, v^d, e^q, e^d) \tag{5.11}$$

where e^{qd} are grid voltages and v^{qd} are voltages applied by the converter at the grids frequency. After linearizing the previous equations, the state-space model will become:

$$\frac{d\Delta x_{lc}}{dt} = A_{lc}\Delta x_{lc} + B_{lc}\Delta u_{lc} \tag{5.12}$$

$$\Delta y_{lc} = C_{lc}\Delta x_{lc} + D_{lc}\Delta u_{lc} \tag{5.13}$$

where A_{lc} and B_{lc} are matrices as defined in 5.8 and 5.9. C_{lc} and D_{lc} matrices will be defined as:

$$C_{lc} = \begin{bmatrix} 0 & 0 & 0 & 0 & 0 & 0 \\ 0 & 0 & 0 & 0 & 0 & 0 \\ 0 & 0 & 0 & 0 & 0 & 0 \\ 0 & 0 & 0 & 0 & 0 & 0 \\ 0 & 0 & 0 & 0 & 0 & 0 \\ 0 & 0 & 0 & 0 & 0 & 0 \\ 0 & 0 & \frac{u_0^q}{U_0} & \frac{u_0^d}{U_0} & 0 & 0 \\ 0 & 0 & \frac{3i_{g0}^q}{2} & \frac{3i_{g0}^d}{2} & \frac{3u_{g0}^q}{2} & \frac{3u_{g0}^d}{2} \\ \frac{3v_{g0}^q}{2} & \frac{3v_{g0}^d}{2} & 0 & 0 & 0 & 0 \end{bmatrix} \tag{5.14}$$

$$D_{lc} = \begin{bmatrix} 0 & 0 & 0 & 0 \\ 0 & 0 & 0 & 0 \\ 0 & 0 & 0 & 0 \\ 0 & 0 & 0 & 0 \\ 0 & 0 & 0 & 0 \\ 0 & 0 & 0 & 0 \\ 0 & 0 & 0 & 0 \\ 0 & 0 & 0 & 0 \\ \frac{3i_{c0}^q}{2} & \frac{3i_{c0}^d}{2} & 0 & 0 \end{bmatrix} \tag{5.15}$$

where u_0^{qc}, u_0^{qd}, i_0^{qc}, i_0^{qd} and U_0 are variables at the linearization point. The linearized state variables will be the form of:

$$\Delta x_{lc} = (\Delta i_c^q, \Delta i_c^d, \Delta u^q, \Delta u^d, \Delta i_g^q, \Delta i_g^d) \tag{5.16}$$

The linearized inputs will be:

$$\Delta u_{lc} = (\Delta v^q, \Delta v^d, \Delta e^q, \Delta e^d) \tag{5.17}$$

The linearized outputs will be:

$$\Delta y_{lc} = (\Delta i_c^q, \Delta i_c^d, \Delta u^q, \Delta u^d, \Delta i_g^q, \Delta i_g^d, \Delta U, \Delta P_u, \Delta P) \tag{5.18}$$

where U represents the voltage magnitude at PCC, P_u is the power going into the AC grid and P is the power going through the converter. All variables with a q or d in the index are variables in the qd reference frame [21]. More details about it can be seen in appendix A.2.

5.3 Phased-Locked Loop (PLL)

The phased-Locked Loop is used to determine the angle (and by consequence the angular speed) of an electric network and to orientate the converter controllers with this angle. A simple PLL scheme can be seen in Figure 5.2.

The three phase PLL consists of a feedback loop that filters the d component of the voltage through a PI regulator. The output of this controller gives the angular

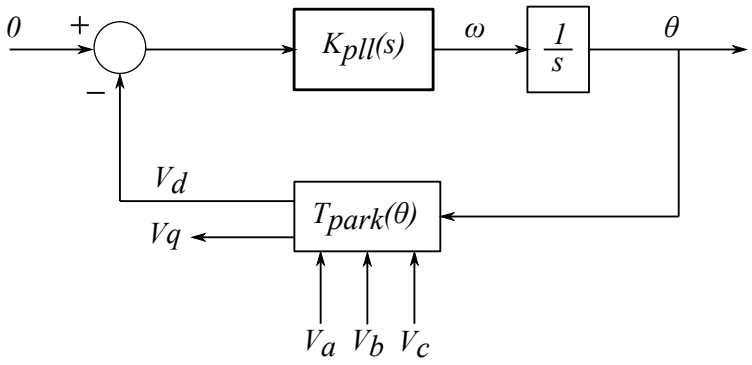

Figure 5.2: Phased Locked Loop

velocity of the grid the integration of this signal gives the angle of the grid which is used for the Park transformations.[8] The PI regulator is:

$$K_{pll} = K_{p-pll} + \frac{K_{i-pll}}{s} \tag{5.19}$$

The method used to determine the gains of this regulator will be presented in the next chapter. The dynamics of the PLL introduce a deviation between the real grid angle and the estimated angle, mostly during voltage transients. To introduce deviation in the converter linear model, the PLL will be linearized as follows:

$$\Delta e_\theta = -\frac{K_{p-pll}s + K_{i-pll}}{s^2 + u_0^q K_{p-pll}s + u_0^q K_{i-pll}}\Delta u^d \tag{5.20}$$

where e_θ represents the difference between the grid angle and the estimated angle by the PLL, that must be included in the model variables. This effect is represented as rotation of the deviation between both angles. By consequence, two synchronous reference frames variables are created: x^{qd}, based on the grid angle and x^{qdc} based on the PLL estimated angle. The relationship between this two references is given by:

$$\Delta x^{qdc} = T_c^{qd}(\Delta x^q, \Delta x^d, \Delta e_\theta)^T \tag{5.21}$$

where T_c^{qd} is the transformation matrix the references, described as:

$$T_c^{qd} = \begin{bmatrix} \cos(e_{\theta 0}) & -\sin(e_{\theta 0}) & -\sin(e_{\theta 0})x_0^q - \cos(e_{\theta 0})x_0^d \\ \sin(e_{\theta 0}) & \cos(e_{\theta 0}) & \cos(e_{\theta 0})x_0^q - \sin(e_{\theta 0})x_0^d \end{bmatrix} \tag{5.22}$$

The inverse transformation is defined as:

$$\Delta x^{qd} = T_c^{qd^{-1}}(\Delta x^{qc}, \Delta x^{dc}, \Delta e_\theta)^T \tag{5.23}$$

where $T_c^{qd^{-1}}$ is:

$$T_c^{qd^{-1}} = \begin{bmatrix} \cos(e_{\theta 0}) & \sin(e_{\theta 0}) & \cos(e_{\theta 0})x_0^q - \sin(e_{\theta 0})x_0^d \\ -\sin(e_{\theta 0}) & \cos(e_{\theta 0}) & -\cos(e_{\theta 0})x_0^q - \sin(e_{\theta 0})x_0^d \end{bmatrix} \tag{5.24}$$

where $e_{\theta 0}$ is the deviation at linearization point and x_0^d and x_0^q are grid oriented variables in qd reference frame at the linearization point [21],[25].

5.4 Current Loop

Current control is a strategy based on vector control that has a decoupling loop and uses to PI regulators to track current references in each axis frame to output voltages in the AC side of the VSC, as seen in Figure 5.3. This loop uses variables

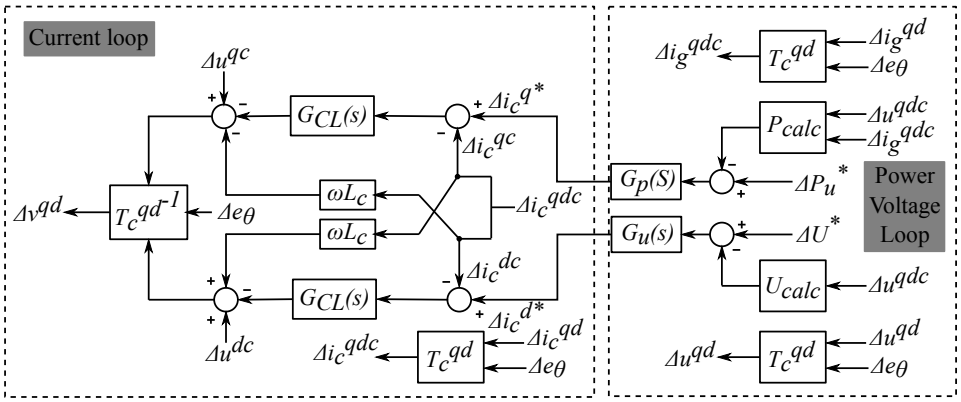

Figure 5.3: Linearized structure of the current, power and voltage loop

calculated from the PLL estimated angle. A more detailed analysis will be given in Chapter 5 [25].

5.5 Power and voltage loop

Power and voltage controllers are conventional PI regulators as seen in Figure 5.3. The feedback signals of these converters must be linearized in order to be included in the model. They are calculated based on x^{qdc} variables [21]:

$$\Delta P_u = \frac{3}{2}(\Delta i_g^{qc} u_0^q + i_{g0}^q \Delta u^{qc} + \Delta i_g^{dc} u_0^d + i_{g0}^d \Delta u^{dc}) \tag{5.25}$$

$$\Delta U = \frac{u_0^q \Delta u^{qc}}{\sqrt{(u_0^q)^2 + (u_0^d)^2}} + \frac{u_0^d \Delta u^{dc}}{\sqrt{(u_0^q)^2 + (u_0^d)^2}} \tag{5.26}$$

5.6 DC grid modeling

The line between the two DC grid terminals, illustrated in Fig.5.4, is used to represent the linear model of the DC system. It is represented using the π equivalent model. The equations for this model are:

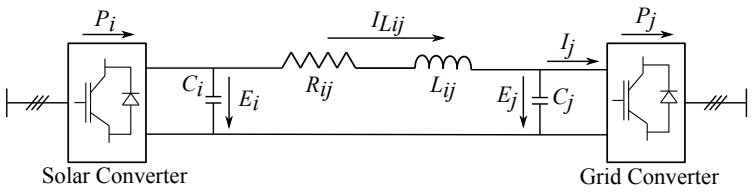

Figure 5.4: DC connection between two nodes of the microgrid

$$\frac{dE_i}{dt} = \frac{1}{C_i}(I_i - I_{Lij}) = \frac{1}{C_i}(\frac{P_i}{E_i} - I_{Lij}) \tag{5.27}$$

$$\frac{dE_j}{dt} = \frac{1}{C_j}(I_{Lij} - I_j) = \frac{1}{C_j}(I_{Lij} - \frac{P_j}{E_j}) \tag{5.28}$$

$$E_i - E_j = R_{ij}I_{ij} + L_{ij}\frac{dI_{Lij}}{dt} \tag{5.29}$$

where E_i and E_j are voltages at the capacitors, I_i and I_j are currents flowing through converters, P_i and P_j are the input and output powers that go through the converters, I_{Lij} is current flowing through the line, R_{ij} and L_{ij} are equivalent resistance and inductance of the line model and C_i and C_j are equivalent capacitances at the sides of the DC link. To include the DC current in the model, it must be linearized as:

$$I_i = \frac{P_i}{E_i} \approx \frac{\Delta P_i}{E_{i0}} - \frac{P_{i0}}{E_{i0}^2}\Delta E_i \tag{5.30}$$

where ΔE_i and ΔP_i are the linearized voltage at bus i and linearized power flowing through converter i. E_{i0} and P_{i0} are variables at linearization point. Based on the grid equations, the linearized state space model of the dc part of the microgrid is

$$\frac{d\Delta x}{dt} = A\Delta x + B_u\Delta u + B_w\Delta w, \quad \Delta y = C_y\Delta x, \quad \Delta z = C_z\Delta x \tag{5.31}$$

where Δx is the vector containing state variables, Δu and Δw are vectors containing controlled and uncontrolled inputs, Δy and Δz are vectors containing controlled and uncontrolled outputs and A, B_u, B_w, C_y and C_z are matrices of suitable dimensions. Usually, in electrical systems, inductor currents and capacitor voltages are used as state variables. Then, the state vector is :

$$\Delta x = (\Delta E_1, ..., \Delta E_n, \Delta E_{n+1}, ..., \Delta E_{n+m}, \Delta I_{L_1}, ..., \Delta I_{L_p})^T \tag{5.32}$$

where n is the number of converters that perform droop control, m is the number of solar plants and p is the number of interconnected branches. The controlled and uncontrolled inputs u and w, and outputs y and z are defined as:

$$\begin{aligned} \Delta u &= (\Delta P_1, ..., \Delta P_n)^T, \quad \Delta w = (\Delta P_{n+1}, ..., \Delta P_{n+m})^T, \\ \Delta y &= (\Delta E_1, ..., \Delta E_n)^T, \quad \Delta z = (\Delta E_{n+1}, ..., \Delta E_{n+m})^T \end{aligned} \tag{5.33}$$

It is worth mentioning that Δu and Δy are controlled variables related to grid converter that controls the DC voltage. Δw and Δz are variables related to solar converter that do not control the DC voltages.

By combining all linear models, the complete structure of the linear model of the microgrid is shown in Figure 5.5.

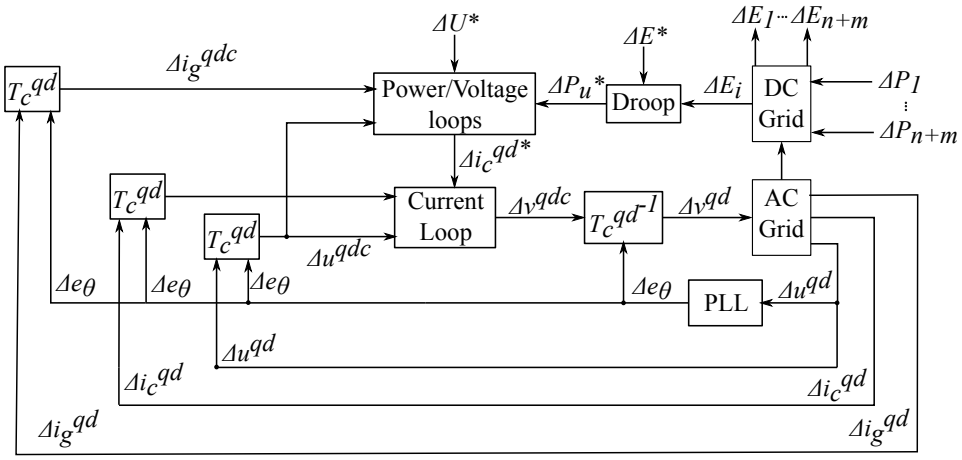

Figure 5.5: Complete linear model of the grid

6. Control Design

This chapter presents the designing procedure for all control loops involved. As presented earlier, the droop control depends on different dynamics including inner control loops in the converter. So a detailed representation of these loops will be presented.

6.1 Current Loop Control

Current loop is a vector control strategy that tracks current references in *qd* frame to give as an output voltages in the AC side of the converter.

Based on the representation of the AC side of the converter the voltage equations can be written similarly as in equation (6.1).

$$\begin{bmatrix} u_q \\ 0 \end{bmatrix} - \begin{bmatrix} v_q \\ v_d \end{bmatrix} = \begin{bmatrix} r_c & l_c\omega_e \\ -l_c\omega_e & r_c \end{bmatrix} \begin{bmatrix} i_q \\ i_d \end{bmatrix} + \begin{bmatrix} l_[c] & 0 \\ 0 & l_c \end{bmatrix} \frac{d}{dt} \begin{bmatrix} i_q \\ i_d \end{bmatrix} \tag{6.1}$$

u_q became 0, because of the PLL and it can be observed that there is coupling between i_q and i_d. In order to control these variables they need to be decoupled and controlled independently. They can be decoupled using:

$$\begin{bmatrix} v_q \\ v_d \end{bmatrix} = \begin{bmatrix} -\hat{v}_q + u_q - l_c\omega_e i_d \\ -\hat{v}_d + l_c\omega_e i_q \end{bmatrix} \tag{6.2}$$

where v_q and v_d are voltages applied by the VSC and $\hat{v}_q$ and $\hat{v}_d$ are output voltages of the current controllers. After applying these changes the equations become:

$$\begin{bmatrix} \hat{v}_q \\ \hat{v}_d \end{bmatrix} = \begin{bmatrix} r_c & 0 \\ 0 & r_c \end{bmatrix} \begin{bmatrix} i_q \\ i_d \end{bmatrix} + \begin{bmatrix} l_c & 0 \\ 0 & l_c \end{bmatrix} \frac{d}{dt} \begin{bmatrix} i_q \\ i_d \end{bmatrix} \tag{6.3}$$

After applying Laplace transformation, the transfer function of the controller will become:

$$\frac{\hat{v}_q(s)}{i_q(s)} = \frac{1}{l_c s + r_c} \tag{6.4}$$

$$\frac{\hat{v}_d(s)}{i_d(s)} = \frac{1}{l_c s + r_c} \tag{6.5}$$

The controller is designed using internal model control (IMC) technique, resulting in the following first order system:

$$G_{CL}(s) = \frac{K_p s + K_i}{s} \tag{6.6}$$

where K_p and K_i constants are defined as:

$$K_p = \frac{l_c}{\tau} \quad K_i = \frac{r_c}{\tau} \tag{6.7}$$

τ represents the time constant is set according to the desired settling time. This represents the time the system needs to stabilize within a range of the final value. The time is set to track the current references within a few milliseconds. To avoid exceeding the maximum current rating of the converter, a saturation scheme is included.

6.2 Power and voltage loop

6.2.1 Structure and functionality

In Figure 6.1, a more explicit control scheme is presented where all control loops are included.Two controllers can be distinguished, the power loop (G_p) which tracks the power reference and and the voltage loop (G_u) that regulates the AC voltage.

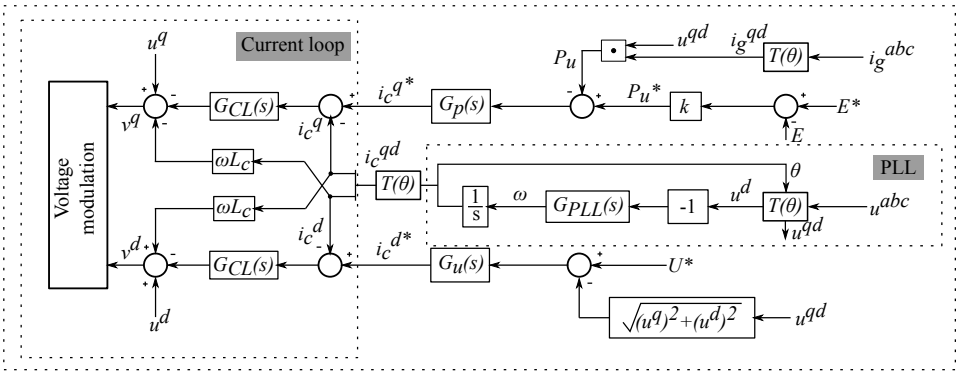

Figure 6.1: Converter control scheme

Since the power loop receives references from the voltage droop, fast dynamics are required to respond to variations in the DC grid. The controller is designed using a procedure called shaping closed-loop transfer functions. This procedure is convenient because it automates the actual controller design, leaving the engineer with the task of selecting bounds ("weights") for the closed loop transfer function. In this case the weight will be the sensitivity function, a very good indicator for the closed loop performance. The requirement for the design is to keep the H_∞ of the weighted sensitivity less than 1 [21].

6.2.2 Terms H_∞ and H_2

The H_∞ norm is a method used to design a controller to stabilize it with a certain performance guaranteed. One of the main advantage of this technique is that it is applicable to multivariate systems that with cross-coupling between channels, but it requires a good model of the system that needs to be controlled [27].

Considering a simple scalar and stable transfer function $f(s)$, the H_∞ norm of this transfer function represents the peak value of $|f(j\omega)|$ as a function of frequency, as expressed in:

$$||f(s)||_\infty = \max|f(j\omega)| \tag{6.8}$$

It is important to mention here that the term *max* does not stand for the maximum value but for the least upper bound. It would be more suitable to replace this term with *sup* but for engineering purpose these terms are the same [26].

The term H_∞ doesn't have any physical meaning, its a pure mathematical whose purpose is to reduce the peak or peaks of one or more transfer functions. The ∞ term suggests the maximum magnitude over the frequency, which can be expressed as:

$$\max|f(j\omega)| = \lim_{p\to\infty}\left(\int_{-\infty}^{\infty}|f(j\omega)|^p d\omega\right)^{\frac{1}{p}} \tag{6.9}$$

Basically what this means is that when we raise $|f|$ to an infinite power, we select the peak value. The term H_∞ comes from the mathematical space over witch the optimization takes place. The H comes from the *Hardy space* of matrix valued functions that are bounded in the open-right half of the complex plane, defined by $Re(s) > 0$. So the H_∞ norm represents the maximum singular value of the function over that space (or the maximum gain at any frequency and in any direction) [26].

In the same manner, H_2 represents the Hardy space of the transfer function $f(s)$, with bounded second norm, which is a set of stable and strictly transfer functions. It can be defined as [26]:

$$||f(s)||_2 = \left(\frac{1}{2\pi} \int_{-\infty}^{\infty} |f(j\omega)|^2 d\omega \right)^{\frac{1}{2}} \tag{6.10}$$

The H_2 norm of a semi-proper (or bi-proper) transfer function (where $\lim_{p\to\infty} f(s)$ is a non-zero constant) is infinite, whereas H_∞ norm is finite [26].

6.2.3 Sensitivity

As mentioned earlier the H_∞ norm of a semi-proper function is used to used to tune a controller to reach a certain performance and stability level. One example of a semi-proper function is the sensitivity function. More details of how to determine the sensitivity transfer function, S, of a closed loop can be found in [26].

The sensitivity transfer function is a very good indicator for evaluating the performance of a closed loop. The goal is to keep S as small as possible and for that its sufficient to consider only the magnitude $|S|$ and ignore its phase. Some specifications regarding S are [26]:

- Minimum bandwidth frequency ω_b^* (the frequency where $|S(j\omega)|$ croses 0.707)
- Maximum tracking error at all selected frequencies
- Maximum steady-state tracking error
- Shape of S in the selected frequency ranges
- Maximum peak magnitude of S (prevents noise amplification at high frequencies)

From a mathematical point of view, these specifications can be concentrated in an upper bound, $\frac{1}{|\omega_p(s)|}$, where $\omega_p(s)$ is a weight selected by the engineer. The P stands for performance, since S is the performance indicator. This requirement becomes:

$$|S(j\omega)| < \frac{1}{|\omega_p(j\omega)|}, \quad \forall\omega \tag{6.11}$$

$$||\omega_p S||_\infty < 1 \tag{6.12}$$

The last equation tells that the H_∞ norm of the weighted sensitivity, $\omega_p S$, must be less than 1 [26].

6.3 Droop control

As described earlier, the droop design must be made considering all dynamics involved in the system because they affect its performance. For this purpose a complete linear model of the system must be employed, which includes all parts that affect the droop operation. Dynamics of the entire system can be seen in Figure 6.2.

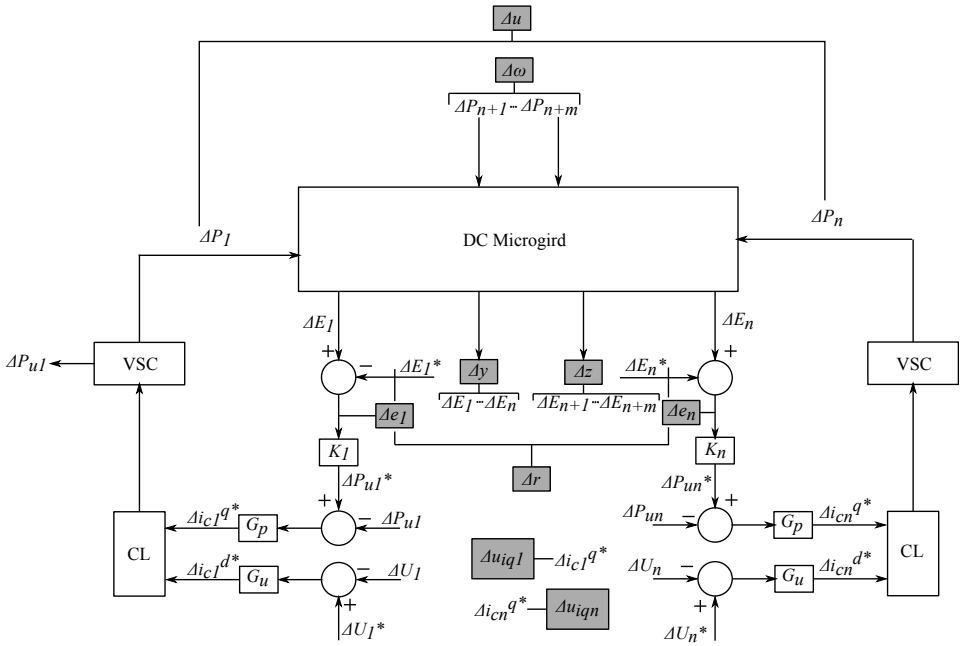

Figure 6.2: DC microgrid control scheme

Before going further with the design procedure, lets see the general structure of a feedback control system and the closed-loop transfer functions.

6.3.1 Closed-loop transfer function

For the purpose of this general analysis, a one degree-of-freedom negative feedback control system will be considered, as described in Figure 6.3.

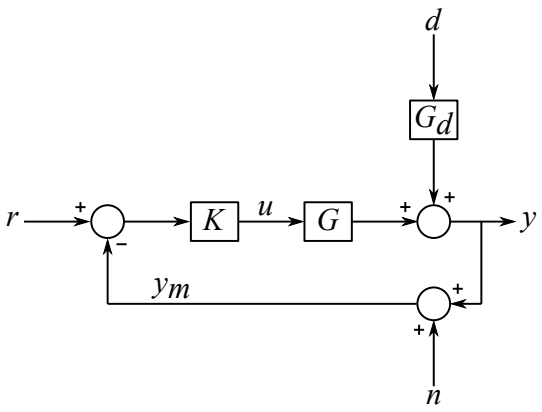

Figure 6.3: Feedback control system [26]

where r represents the reference signal set for the output signal of the controller y; d is the disturbance and n is the measurement noise. The input into the plant model G will be:

$$u = K(s)(r - y - n) \tag{6.13}$$

where K is the actual controller. The purpose is to design K in such a way that to keep the error e as small as possible:

$$e = y - r \tag{6.14}$$

Considering also the disturbances, the plant model can be defined as:

$$y = G(s)u + G_d(s)d \tag{6.15}$$

Considering the input defined in equation 6.13 the plant model can be rewritten as:

$$y = GK(r - y - n) + G_d d \tag{6.16}$$

$$(I + GK)y = GKr + G_d d - GKn \tag{6.17}$$

Based on this equation the closed loop response is defined as:

$$y = (I + GK)^{-1}GKr + (I + GK)^{-1}G_d d - (I + GK)^{-1}GKn \tag{6.18}$$

where

$$(I + GK)^{-1}GK = T \quad \text{and} \quad (I + GK)^{-1} = S \tag{6.19}$$

We can see that $T + S = I$. Using this information, the error e and the plant input signal u can be written as:

$$e = y - r = -Sr + SG_d d - Tn \tag{6.20}$$

$$u = KSr - KSG_d d - KSn \tag{6.21}$$

The following notation is defined, based on [26]:

- $L = GK$ loop transfer function
- $S = (I + GK)^{-1} = (I + L)^{-1}$ sensitivity function
- $T = (I + GK)^{-1}GK = (I + L)^{-1}L$ complementary sensitivity function

The sensitivity function S is the closed-loop transfer function from disturbance outputs to the system outputs, and its complementary T is the closed-loop transfer function from the reference to the output [26].

The name "sensitivity" for the function S has first been given by Bode because it shows the relative sensitivity of T to the relative plant model error. For a certain frequency, in a SISO (single input single output) plant this can be mathematically defined as:

$$\frac{dT/T}{dG/G} = S \tag{6.22}$$

In a more general manner, the closed loop transfer function of a SISO system with a negative feedback can be expressed as:

$$\text{OUTPUT} = \frac{\text{"direct"}}{1 + \text{"loop"}}\text{INPUT} \tag{6.23}$$

where "direct" is the transfer function of the direct effect of the input to the output and "loop" is the transfer function around the loop [26].

6.3.2 Droop design

For design purpose Figure 6.2 will be redrawn as in Figure 6.4 in a feedback structure to identify all closed loop functions. All closed-loop transfer functions

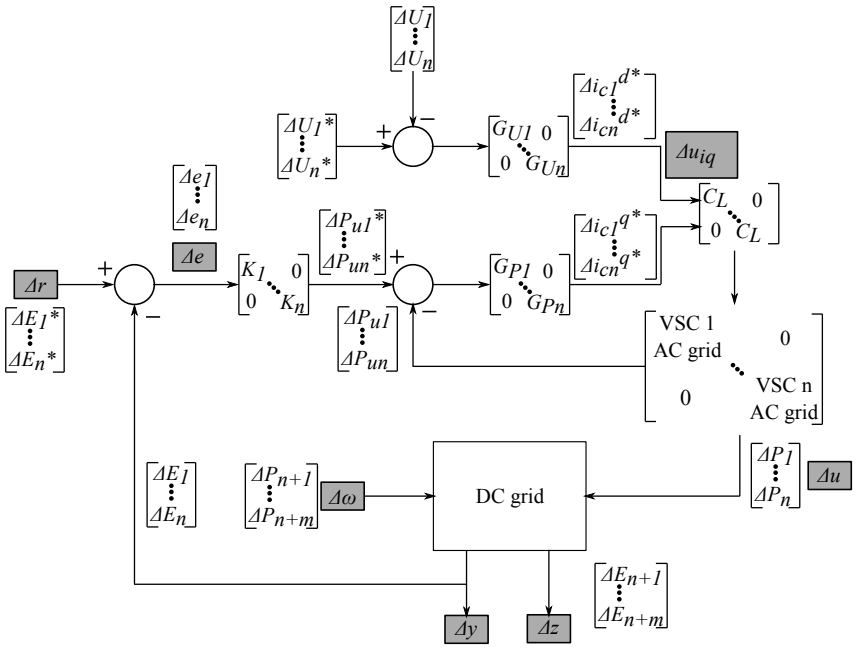

Figure 6.4: DC microgrid control structure

can be written, considering all grid dynamics, as [21]:

$$\begin{aligned}
\Delta e(s) &= \Delta y(s) - \Delta r(s) = (E_s(s)E_r(s))\Delta v(s) \\
\Delta u_{iq}(s) &= (U_s^{u_{iq}}(s)U_r^{u_{iq}}(s))\Delta v(s) \\
\Delta v(s) &= (\Delta s(s)\Delta r(s))^T \\
\Delta r(s) &= (\Delta E_1^*, ..., \Delta E_n^*)^T \\
\Delta u_{iq}(s) &= (\Delta i_{c1}^{q*}, .., \Delta i_{cn}^{q*})^T
\end{aligned} \tag{6.24}$$

$E_r(s)$ and $E_s(s)$ are transfer function matrices related to droop references, r and power injected by the solar plant into the grid s, with voltage errors at the controlled points. In a similar manner, $U_s^{u_{iq}}(s)$ and $U_r^{u_{iq}}(s)$ are matrices related to droop references and solar power but with the active current loop reference for the controlled converters.

The most suitable way to design the droop control is to perform a frequency analysis on the transfer functions of the MIMO (Multiple Input Multiple Output) system using singular value representation, or SVD (more details about it in appendix). For different droop controllers some requirements must be defined to obtain the appropriate response. Usually these are:

- Desired power sharing between converters that control the voltage;
- Maximum voltage deviation allowed at grid terminals;
- Maximum deviation above the converters' power rating;

Usually these requirements are transformed as gain boundaries in the frequency response of the multivariable system. The structure of the droop control can be defined as:

$$K = \begin{bmatrix} K_1 & 0 & ... & 0 \\ 0 & K_2 & ... & 0 \\ 0 & 0 & ... & K_n \end{bmatrix} \tag{6.25}$$

where K_1 to K_n are droop constants each of the VSCs. For a dynamic analysis, K_n must be selected using certain tunning techniques [21].

Based on requirements described above, the singular values of the transfer function matrices of the system can be defined as:

$$\sigma_i(G(j\omega)) = \sqrt{\lambda_i(G^T(j\omega)G(j\omega))} \tag{6.26}$$

where λ_i represents the eigenvalue of $G^T(j\omega)G(j\omega)$ matrix, and G^T is the complex conjugate transpose of G.
Singular values are also named sometimes principal values or principal gains and the associated directions are called principal directions. Basically these singular values show how the input vector of the system is seen at the output. Also the input and output directions are related through the singular values [21].

Another method that could be used is eigenvalue decomposition but there are some advantages of SVD that make them more suitable:

- Singular values give better information of the plants gains;
- Plant directions obtained from SVD are orthogonal;
- SVD can also be applied to non-square plants;

The maximum singular value ($\bar{\sigma}(G(j\omega))$) is interesting to be analyzed because it can show the maximum peak of an input vector oscillating at a certain frequency. This analysis could be extended to a range of frequencies, obtaining the SVD representation of a transfer function matrix. So, assuming a predefined power sharing between converters the only limitations imposed are by the voltage error and the converter current rating. These limitations are imposed as boundaries on the SVD response that basically limits the value of K_g [21].

As mentioned before, $|S(j\omega)|$ gives useful information about the controllers performance. The maximum error e caused by an input reference r is given by:

$$\max_{r\neq 0} \frac{||e||_2}{||r||_2} = \max_{\omega} \bar{\sigma}(S(j\omega)) \tag{6.27}$$

So to reduce any disturbances caused by the solar plant s in the voltage error e can be understood as minimizing

$$\bar{\sigma}(E_s(s), E_r(s)) \tag{6.28}$$

and keeping the current flowing through the converter within the limits can understood as:

$$\bar{\sigma}(U_s^{u_{iq}}(s), U_r^{u_{iq}}(s)) \tag{6.29}$$

7. Case Study

7.1 Proposed System

As mentioned before this thesis proposes a power based voltage droop control strategy for generic DC microgrids. For the analysis, a three terminal microgrid system has been proposed, but this control strategy can easily be applied to any multiterminal configuration with some minor changes. This system has a 10 kW photovoltaic (PV) plant which is connected, through two AC-DC converters (VSCs), to the AC grid at two different connection points, as it can be seen in the Figure 7.1.

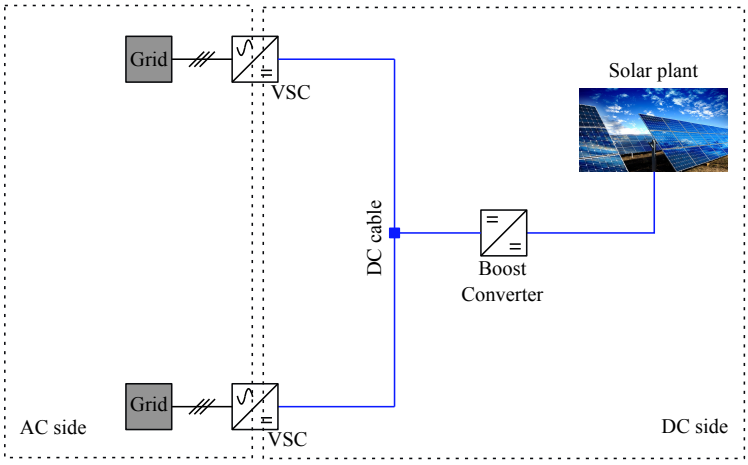

Figure 7.1: Case study DC microgrid

The two voltage source converters (VSC1 and VSC 2), that are connected to two different AC grid points but under similar conditions, carry the droop voltage control. The converter connected to the solar plant boosts the output voltage of the plant and injects the power in the grid. No control strategy will be applied to this converter so, the analysis will be focused on the two VSCs.

The AC grid will be modeled as a three-phase voltage source connected to a grid Thevenin equivalent (as seen in Figure 5.1). For the VSCs, static model will be used where the AC and the DC sides are separated but connected through a power link. DC cables are represented by the classical PI model. Since the focus of this thesis is on the control strategy, the PV plant will be modeled as a simple current source connected in parallel with a capacitor.

The parameters used for this analysis are shown in Tables 7.1 and 7.2.

Considering all components in the model, that have been described before, a sequential design methodology for all controllers involved will be presented. Since the droop performance is affected not only by AC and DC grid dynamics but also by the other controllers dynamics. Thus, inner control loops, current loop, power loop and voltage loop design will be presented and their dynamics will be furthered considered in the droop tunning process.

Table 7.1: AC parameters

AC parameters	Values	Units
AC line to line nominal voltage	400	V
Frequency	50	Hz
VSCs nominal powers P_1 and P_2	10	kVA
Coupling inductance L_c	5.4	mH
Coupling resistance R_c	0.5	Ω
Filter capacitance C_f	4.7	μF
Grid Thevenin ratio R_n/X_n	0.9	-

Table 7.2: DC parameters

DC parameters	Value	Unit
line resistance R	1	Ω
line inductance L	0.2	mH
DC link capacitors C_{DC}	1020	μF
Reference Voltage E_{DC}	800	V

7.2 Linear model

The system analysis and controllers design will be based on the linear model and a comparison with the non-linear model will be performed.

The linear model of the AC system (for both converters) is derived based on the diagram described in Figure 5.1. Then the state space model will be the one described by equations (5.12) and (5.13).

Once the AC model is determined, the DC grid state space is derived (similar as equation (5.31)). The defined state variables Δx, input signals Δu and Δw, and output signals Δy and Δz are:

$$\Delta x = (E_1, E_2, E_3, I_{L13}, I_{L23}) \tag{7.1}$$

$$\Delta u = (\Delta P_1, \Delta P_2) \quad \Delta w = (\Delta P_3) \tag{7.2}$$

$$\Delta y = (\Delta E_1, \Delta E_2 \quad \Delta z = (\Delta E_3) \tag{7.3}$$

and the linearized state space matrices are:

$$A = \begin{bmatrix} -\frac{P_{10}}{C_1 E_{10}^2} & 0 & -\frac{1}{C_1} & 0 & 0 \\ 0 & -\frac{P_{20}}{C_1 E_{20}^2} & 0 & 0 & \frac{1}{C_2} \\ 0 & 0 & \frac{P_{30}}{C_1 E_{30}^2} & \frac{1}{C_3} & \frac{1}{C_3} \\ \frac{1}{L_{13}} & -\frac{1}{L_{13}} & -\frac{R_{13}}{L_{13}} & 0 & \\ 0 & \frac{1}{L_{23}} & -\frac{1}{L_{23}} & 0 & -\frac{R_{23}}{L_{13}} \end{bmatrix} \tag{7.4}$$

$$B_u = \begin{bmatrix} \frac{1}{C_1 E_{10}^2} & 0 \\ 0 & \frac{1}{C_2 E_{20}^2} \\ 0 & 0 \\ 0 & 0 \\ 0 & 0 \end{bmatrix} \quad B_w = \begin{bmatrix} 0 \\ 0 \\ \frac{1}{C_3 E_{30}} \\ 0 \\ 0 \end{bmatrix} \tag{7.5}$$

$$C_y = \begin{bmatrix} 1 & 0 & 0 & 0 & 0 \\ 0 & 1 & 0 & 0 & 0 \end{bmatrix} \quad C_z = \begin{bmatrix} 0 & 0 & 1 & 0 & 0 \end{bmatrix} \tag{7.6}$$

After determining the complete linear model of the system, all controllers will be designed.

7.3 Phase Locked Loop (PLL)

The PLL is used to determine the angular velocity of the grid and to synchronize the AC side of the VSC with the grid frequency. This is done using a PI regulator whose proportional gain (K_p) and integral gain (K_i) are determined based on the amplitude of the AC voltage $V_{peak} = 326.6$V and the damping ratio which is set to $\xi = 0.707$. Then the gains are calculated using equations 7.7 and 7.8, derived from [8].

$$K_{p-pll} = \frac{\xi \cdot 2 \cdot \omega}{V_{peak}} \tag{7.7}$$

$$K_{i-pll} = \frac{\omega^2}{V_{peak}} \tag{7.8}$$

7.4 Current Loop

The current loop is based on a vector control strategy in the synchronous reference frame, tuned by an IMC control technique. This control loop is made of two identical PI controllers with a decoupling loop, to track the reference currents in the *qd* frame in a certain time τ. The controller gains are calculated based on equation 6.7. $\tau = 1$ms is the control time constant. This time constant must be chosen considering converters restriction (it should be faster than converters switching frequency) but since here it is used a static model for the converter, this particular issue is not of interest.

Figure 7.2 shows a comparison between the linear and nonlinear model (derived based on system equations) of the current loop response. It can be clearly seen that the current responds accordingly to the reference change and stabilizes within the current set time.

7.5 Power Loop

To track power references, a conventional PI controller is used. As seen in Figure 6.1, the power loop is getting its input reference from the droop voltage loop. To avoid large deviations of the DC voltage this controller needs a fast response time. This is obtained using optimization robust control technique.

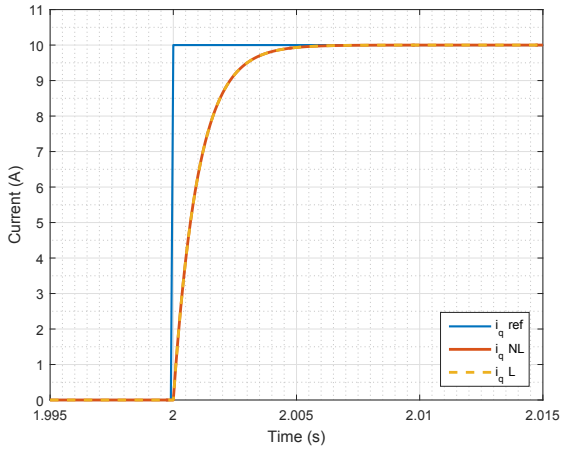

Figure 7.2: Current loop response. Comparison between linear and non-linear model

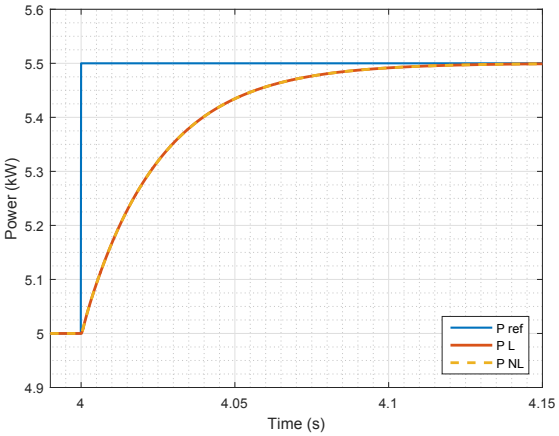

Figure 7.3: Power loop response. Comparison between linear and non-linear model

The settling time for the power controller has been set to 100 ms. Fig 7.3 shows the response for the power loop for both linear and non-linear models, both of them matching, validating the design process.

7.6 Voltage Loop

To regulate the AC voltage, another controller is used. This is designed in the same manner as the power loop. The voltage loop response is shown in Figure 7.4.

7.7 Voltage Droop Control

The droop control is designed considering all systems dynamics. This is done based on the linear model determined earlier. The complete linear model of the case study can be seen more detailed in Figure 7.5.

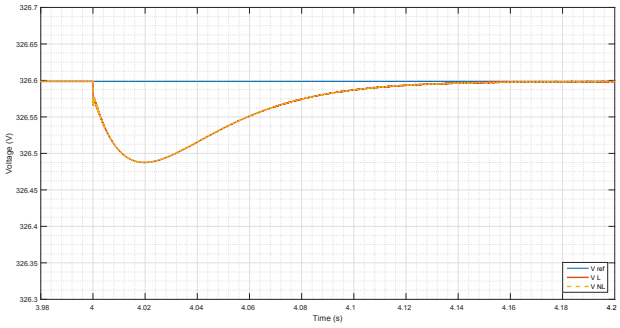

Figure 7.4: Voltage loop response. Comparison between linear and non-linear model

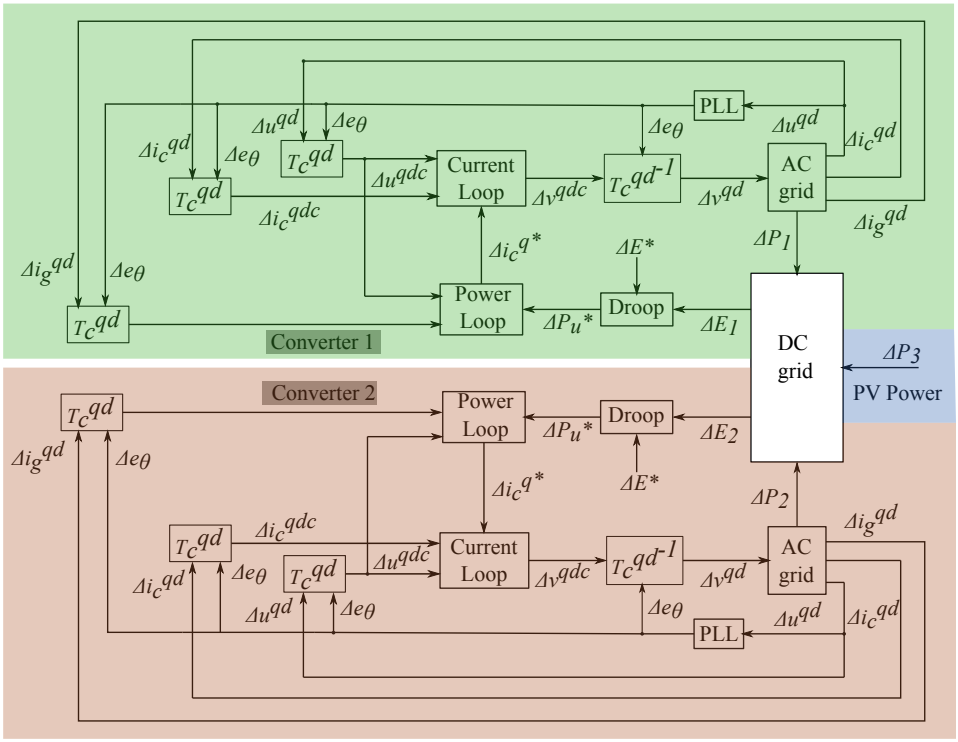

Figure 7.5: Case study DC microgrid

After the linear model is derived some specifications are established for the control design:

- Equal power sharing between converters;
- A 10% maximum DC voltage deviation;
- A 10% maximum transient power is allowed over the power rating of the converter to avoid over currents;

To include these requirements in the droop design, a frequency analysis will be performed to find the best droop constants that meet these specifications. This is done by imposing gain limitations on the frequency response of the selected transfer functions of the system.

Since its a MIMO system, the SVD technique is used to get the maximum gains. Based on the generic feedback control system described in Fig.6.3, where the disturbance d is the output power of the PV plant P_{PV} (which changes at a certain specified time.), the plants input signals u are the reference powers for the two converters (P_{ref1} and P_{ref2}) and e represents the voltage errors at the droop controlled buses (e_1 and e_2) two transfer functions that are to be analyzed are determined based on equations 6.20 and 6.21. The noise is 0 since its not considered in this analysis and the reference is assumed to be constant so, the transfer functions that are to be analyzed, are described in Figure7.6 and Figure 7.7.

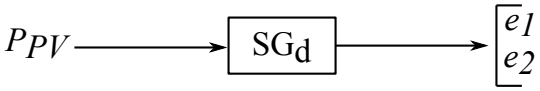

Figure 7.6: First transfer function

Figure 7.7: Second transfer function

Knowing the allowed voltage deviation, the gain limit imposed to the frequency response of the first transfer function (TF1) can be calculated as:

$$\begin{aligned}\bar{\sigma}(TF1(0)) \leq \frac{||e(0)||_2}{||w(0)||_2} &= 20\log_{10}\frac{\sqrt{(e_{max1}^2+e_{max2}^2}}{P_{maxPV}} \\ &= 20\log_{10}(\frac{\sqrt{(800\cdot 0.1)^2\cdot 2}}{(10\cdot 10^3)}) = -38.92dB\end{aligned} \tag{7.9}$$

where e_{max1} and e_{max2} are maximum voltage deviations and P_{maxPV} is the maximum PV power input.

In a similar manner the gain limit for the frequency response of the second transfer function (TF2) is:

$$\begin{aligned}\bar{\sigma}(TF2(0)) \leq \frac{||u(0)||_2}{||w(0)||_2} &= 20\log_{10}\frac{\sqrt{(P_{ref1}^2+P_{ref2}^2)}}{P_{maxPV}} \\ &= 20\log_{10}(\frac{\sqrt{(10\cdot 10^3\cdot 1.1)^2\cdot 2}}{(10\cdot 10^3)}) = 3.83dB\end{aligned} \tag{7.10}$$

These constraints can be extended or narrowed with the frequency because of the power loop limitations. It is assumed that it cannot act over 40 rad/s. Thus, the constraint of the first transfer function can be "relaxed" allowing error deviations at frequencies higher than 40 rad/s. The second transfer function is limited to avoid acting with the power loop over 40 rad/s. These constraints can be seen in the Fig.7.8

After the requirements are established, the controller can be tuned accordingly. The power is shared equally between the two converters, requirement which is imposed by the system design. The droop controller for our multi-variable system is

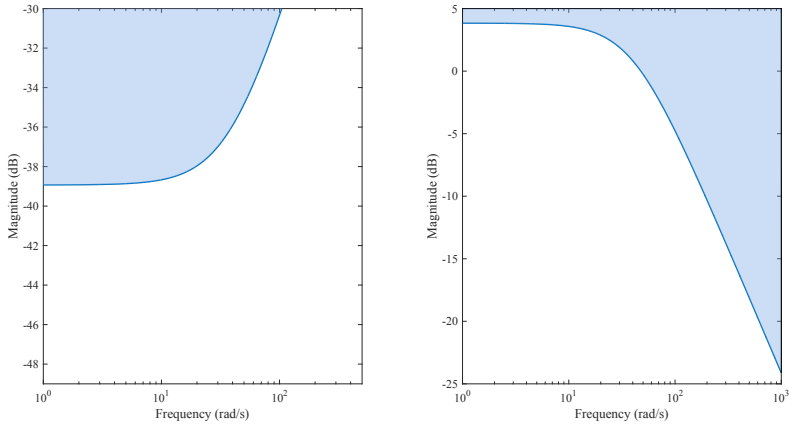

Figure 7.8: Frequency constraints for TF1 and TF2

defined as:

$$K = \begin{bmatrix} K_1 & 0 \\ 0 & K_2 \end{bmatrix} \tag{7.11}$$

Considering the areas defined in Fig.7.8, an optimization routine is performed to find the best droop constants that fulfill both requirements. The power limitations is set as a hard requirement to avoid exceeding rated currents in the converter whereas the error limitation is set as a soft requirement, for the optimization tool. This tool is able to optimize both K_1 and K_2 to match the specifications. The optimization gives a value of 85 W/V for the droop controllers, to ensure that the system meets the criteria as seen in Fig.7.9

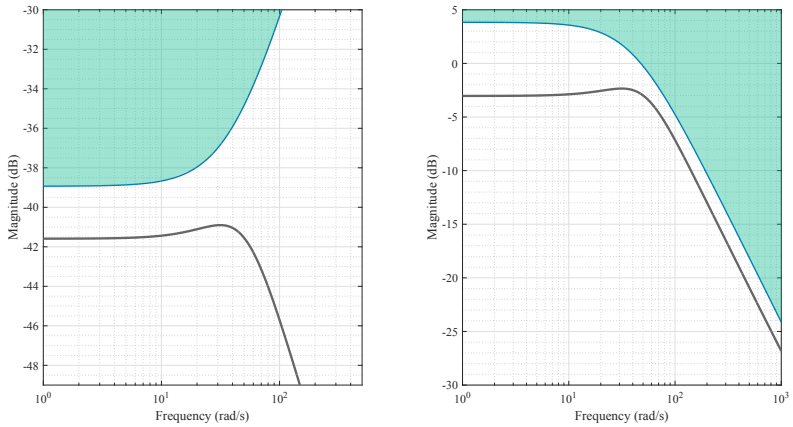

Figure 7.9: Frequency constraints for TF1 and TF2

7.8 System response

To confirm the design of the droop control, simulation of the entire system will be performed to show the system response to a change of injected power by the PV to a 10% of the nominal value. This is done to replicate the system behavior due to a change in the solar output caused by the intermittent nature of solar radiation.

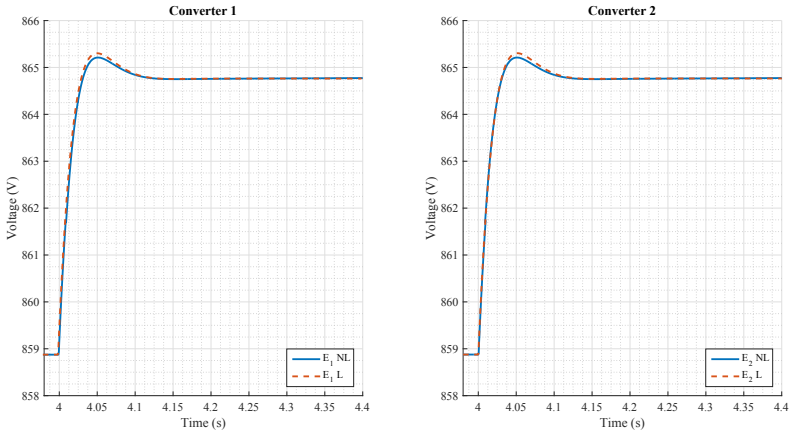

Figure 7.10: Voltage response due to power step change

Figure7.10 shows the DC voltage response due to power step change in the PV output. It can be seen that the voltage stays within the limits imposed in the droop design (10% of nominal voltage) . Also the the linear and non linear models present similar dynamics, confirming that the linear model is suitable for the droop design.

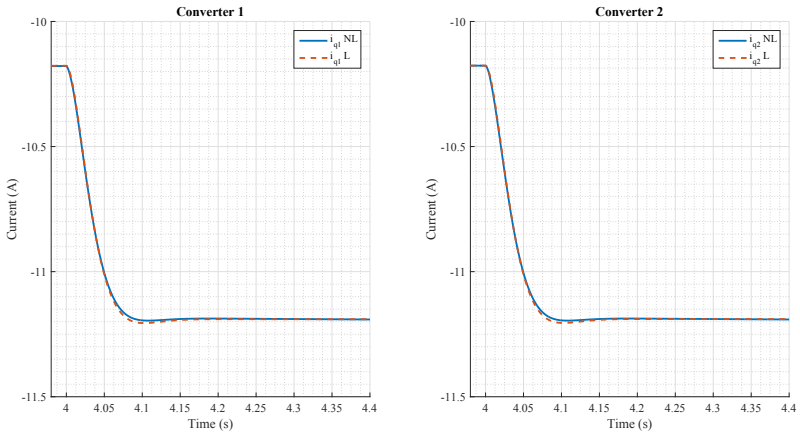

Figure 7.11: AC currents in qd frame response due to power step change

Figure 7.11 shows AC currents (in qd frame) when the power step change occurs. Linear and non linear model have a similar behavior.

Powers in the two converters can be observed in Figure 7.12. It can be observed the equal power sharing between converters (imposed by system design). Also linear and non-linear have a similar similar behavior.

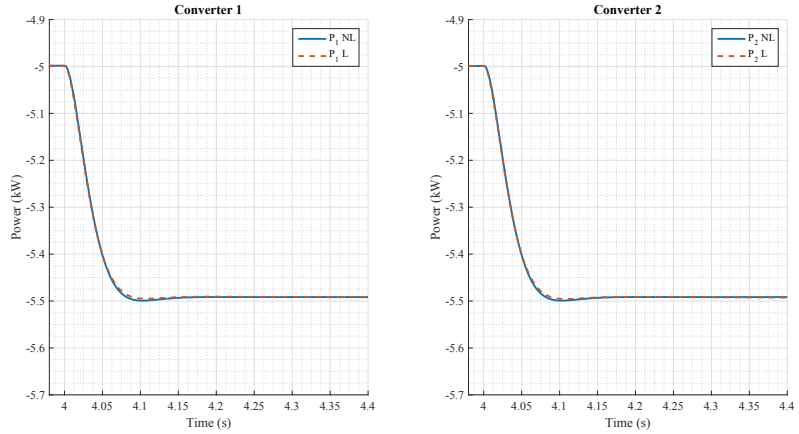

Figure 7.12: Converters power response due to power step change

A new simulation is performed to observe the grid response to a PV step change form 0 to the nominal value of 10 kW. Figures 7.13, 7.14 and 7.15 show the grid response to the PV step change. This also confirms the design of the droop controller. Large over-voltages and over-currents are avoided in the grid considering that the step change is even more aggressive.

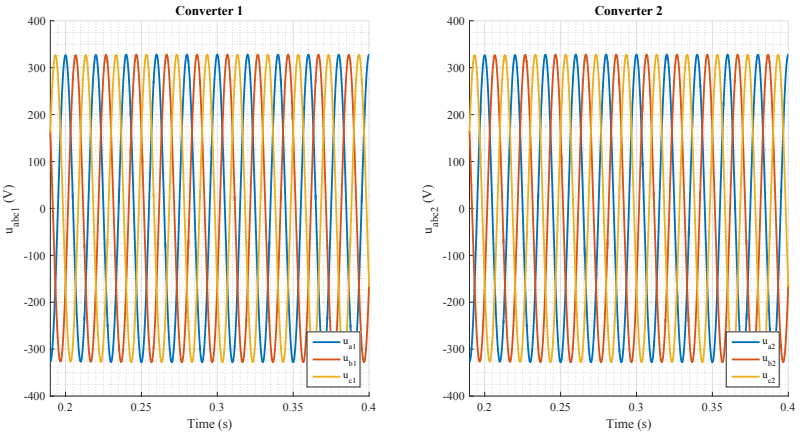

Figure 7.13: Grid voltages in abc frame

The system response can be seen in Figure 7.16. In the second chart, the equal power sharing between the converters can be observed. The slight difference between the voltage at the VSCs terminals and the voltage at the PV terminal represents the voltage drop across the cable.

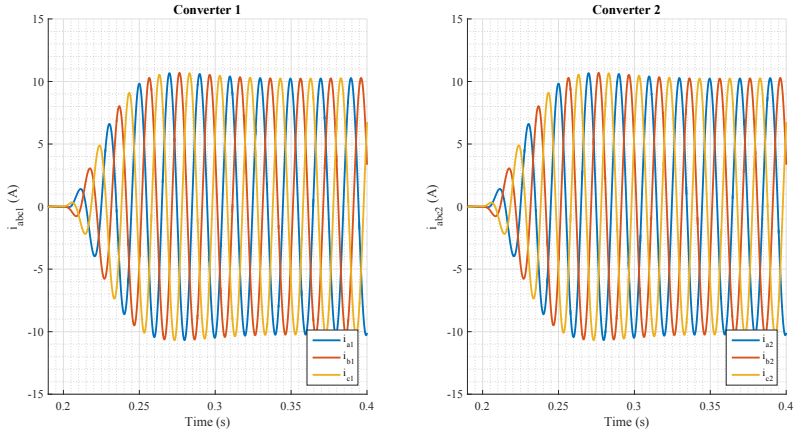

Figure 7.14: Grid currents response to power step change

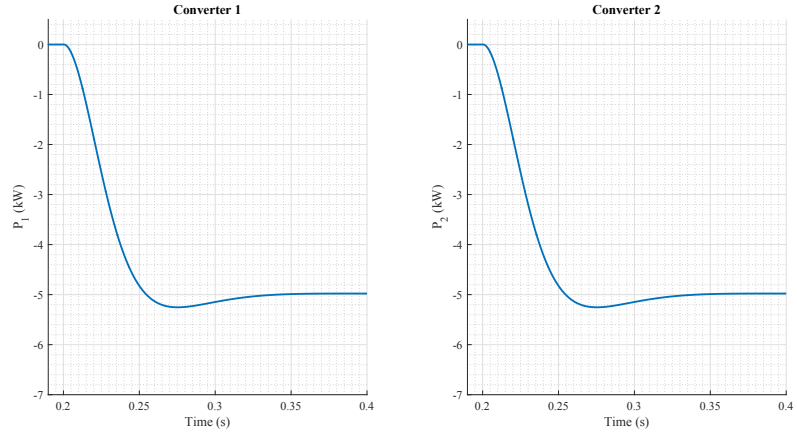

Figure 7.15: Grid power response to power step change

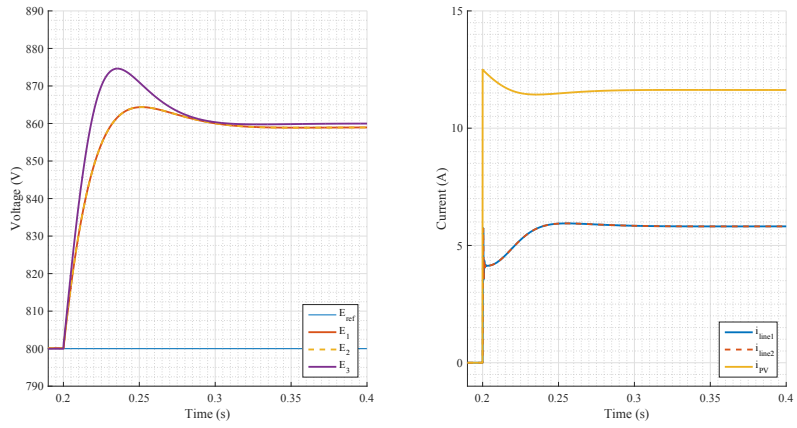

Figure 7.16: System response to power step change

8. Cost-Benefit Analysis of DC Microgrid

The following analysis aims to compare costs involved in AC and DC microgrid solutions. For this purpose a hypothetical scenario is considered described as follows.

A small industrial facility, somewhere in United States, wants to take advantage of its position with high solar radiation and to make an investment in a PV system that will inject all the power into the grid. This company wants to install 30 kW of solar panels on their rooftop, which will be connected to the AC grid in two different points . They want to maximize their profit during the operation of the plant (10 years) with the possibility of extending it for another 10 years.

Two solutions are proposed for connecting the PV system to the grid: through an AC microgrid and a DC microgrid. Even though they are aware of technical differences and difficulties, they want to know which solution is more attractive from a financial perspective.

After a preliminary climate analysis of the sight, the company realized the it rarely rains in the area and the solar radiation is high and mostly constant from one day to another (especially during summer). Considering historical climate data, they forecasted capacity factor during each period for this 10 year horizon as described in Table 8.2

Table 8.1: Forecasted capacity factor

	T=1	T=2	T=3	T=4	T=5	T=6	T=7	T=8	T=9	T=10
%	34.5	35.2	36	35.8	35	34.7	34.9	34	35	35.3

Also, after a market analysis they realized that the electricity price reflects the daily peak-valley profile of demand.Based on historical data regarding the electricity price [28], an increment of about 3% per year is selected. The electricity price, at the beginning of the project, is 10.48 cents/kWh.[29]

Considering the fact that there are other sources in the area, the electricity demand is fairly limited. So this solar plant can have some curtailment periods. But for the upcoming years it is predicted that this demand will increase with approximately 3.5% per year.The current demand is around 60 MWh/year

8.1 AC microgrid

The first solution proposes to install the PV using an AC microgrid as described in Fig.8.1.

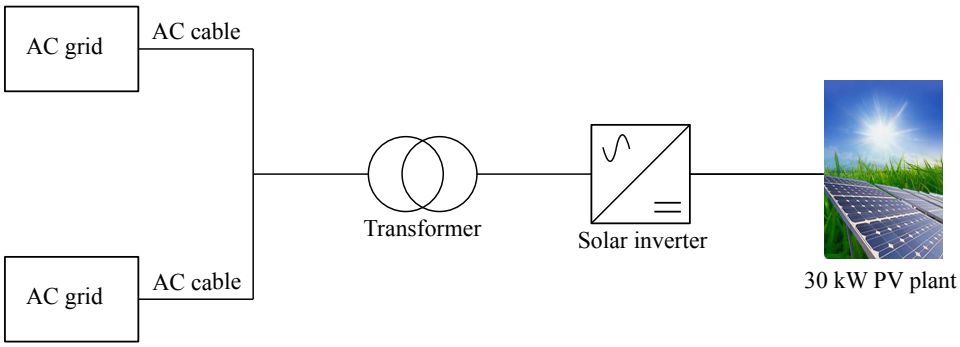

Figure 8.1: AC microgrid solution

The elements that make the object of initial investment, based on the schematic in Fig.8.1 are: PV modules, inverter, AC cable and transformer. On top of that labour costs and other taxes (such as grid connection tax) are added. Based on [30] the cost for a PV module is estimated at 0.64$/W, the inverter is 0.13$/W, labor and other equipments are 0.15$/W and taxes are 0.03$/W. The AC cable is provided by [31]. The transformer cost is based on [32]. All costs are centralized in Table 8.2 making a total investment cost of 40754$

Table 8.2: AC microgrid costs

Element	Cost(euros)
PV module	19200
Inverter	3900
Labor and equipment	4500
AC cable	10554
Transformer	1700
Taxes	900

The transformer is used as a galvanic isolation (requirement imposed by the TSO). For this solution operating and maintenance costs are assumed to be around 400$ per year. They represent a worker hired for some working hours during the year. The operating costs are assumed to be proportional with the sold energy, monetizing the energy losses. They are assumed to be 1 % of the total energy produced. The facility owners will consider a discount rate of 5 %. The cost benefit analysis can be seen in detail in the Table 8.4.

8.2 DC microgrid

The second solution is to install the PV panels using a DC microgrid configuration:

Elements that make the object for the initial investment are: PV modules, converter, DC cable, and two transformers for galvanic isolation. Also taxes and labor costs are added. These, together with the PV module and the converter have the same price structure as in the previous case. The DC cable solution is provided by [33]. These cables are specially designed for solar industry. The same transformer

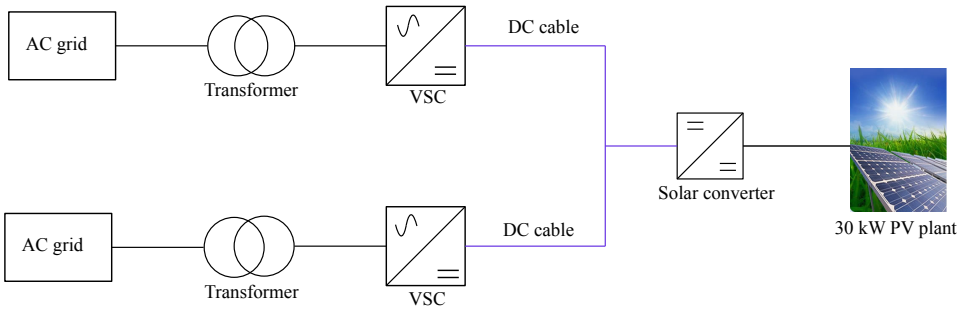

Figure 8.2: DC microgrid solution

is considered as in the previous case. The only difference is that in this system two transformers are used. All costs are centralized in Table 8.3.

Table 8.3: DC microgrid costs

Element	Cost(euros)
Module	19200
Converter	3900
Labor and equipment	4500
Taxes	900
DC cable	1925
Transformers	3400
VSCs	3360

For the DC microgrid solution the maintenance costs are assumed to be the same as before (400 euros per year). The operating costs are assumed to be proportional with the sold energy, monetizing energy losses. In this case it is technically proven that DC microgrid systems have lower overall losses. According to [34] overall loses in DC compared to AC systems are 8 % lower. So considering this, they are assumed to be 0.92% of the total energy produced.

The discount rate will be similar, 5% and the total investment cost is summed up to 37185$.The cost benefit analysis can be seen in detail in the Table 8.5.

8.3 Results

All informations in tables 8.4 and 8.5 are calculated based on the formulas in the seminar [35]. By using the AC microgrid the company would an internal rate of return (IRR) of 14% whereas with the DC solution, the IRR would be 16% making it a more desirable solution. Payback for both solutions is sometime between year 6 and year 7.

Table 8.4: Cost benefit analysis AC microgrid

Alternative A/Period	0	1	2	3	4	5	6	7	8	9	10
Installed power (kW)	30	30	30	30	30	30	30	30	30	30	30
Energy price yearly increase rate	0.03	0.03	0.03	0.03	0.03	0.03	0.03	0.03	0.03	0.03	0.03
Energy price ($/kWh)	0.1048	0.1079	0.1112	0.115	0.118	0.121	0.125	0.1289	0.1328	0.1367	0.1408
Initial investment ($)	40754										
Fix costs ($/year)	400	400	400	400	400	400	400	400	400	400	400
Variable costs (%of energy sold)	0.01	0.01	0.01	0.01	0.01	0.01	0.01	0.01	0.01	0.01	0.01
Energy demand yearly increase rate	0.03	0.03	0.03	0.03	0.03	0.03	0.03	0.03	0.03	0.03	0.03
Demand (kWh)	60000	61800	63654	65564	67531	69556	71643	73792	76006	78286	80635
Discount rate	0.05	0.05	0.05	0.05	0.05	0.05	0.05	0.05	0.05	0.05	0.05
Period	0	1	2	3	4	5	6	7	8	9	10
Capacity factor		0.345	0.352	0.36	0.358	0.35	0.347	0.349	0.34	0.355	0.35
Available energy (kWh)		90666	92506	94608	94082	91980	91192	91717	89352	93294	91980
Energy generated (kWh)		61800	63654	65564	67531	69556	71643	73792	76006	78286	80635
Demand (kWh)	60000	61800	63654	65564	67531	69556	71643	73792	76006	78286	80635
Energy to be sold without losses (kWh)		61182	63017	64908	66855	68861	70927	73055	75246	77504	79829
Receipts ($)	0	6604.2	7006.4	7433	7885.8	8366	8876	9416.1	9989.5	10598	11243
Investments ($)	40754										
Fix costs ($)	400	400	400	400	400	400	400	400	400	400	400
Energy losses (kWh)		618	636.54	655.6	675.31	695.6	716.4	737.92	760.06	782.86	806.35
Variable costs (energy losses) ($)		66.709	70.772	75.08	79.655	84.51	89.65	95.112	100.9	107.05	113.57
Total payments	40754	466.71	470.77	475.1	479.65	484.5	489.7	495.11	500.9	507.05	513.57
Cash flow ($)	-40754	6137.5	6535.7	6958	7406.1	7882	8386	8920.9	9488.6	10091	10730
Acumulated Cash flow ($)	-40754	-34616	-28081	-21123	-13717	-5835	2551	11472	20960	31051	41781
Actualized cash flow ($)	-40754	5845.3	5928	6011	6093.1	6175	6258	6339.9	6422.2	6504.6	6587.1
Acumulated actualized cash flow ($)	-40754	-34909	-28981	-22970	-16877	-10702	-4444	1896	8318.2	14823	21410

Table 8.5: Cost benefit analysis DC microgrid

Alternative A/Period	0	1	2	3	4	5	6	7	8	9	10
Installed power (kW)	30	30	30	30	30	30	30	30	30	30	30
Energy price yearly increase rate (%)	0.03	0.03	0.03	0.03	0.03	0.03	0.03	0.03	0.03	0.03	0.03
Energy price ($/kWh)	0.1048	0.10794	0.11118	0.11452	0.118	0.1215	0.1251	0.1289	0.1328	0.13674	0.14084
Initial investment ($)	37185										
Fix costs ($/year)	400	400	400	400	400	400	400	400	400	400	400
Variable costs (%of energy sold)	0.0092	0.0092	0.0092	0.0092	0.0092	0.0092	0.0092	0.0092	0.0092	0.0092	0.0092
Energy demand yearly increase rate	0.03	0.03	0.03	0.03	0.03	0.03	0.03	0.03	0.03	0.03	0.03
Demand (kWh)	60000	61800	63654	65563.6	67531	69556	71643	73792	76006	78286.4	80635
Discount rate	0.06	0.06	0.06	0.06	0.06	0.06	0.06	0.06	0.06	0.06	0.06
Period	0	1	2	3	4	5	6	7	8	9	10
Capacity factor		0.345	0.352	0.36	0.358	0.35	0.347	0.349	0.34	0.355	0.35
Available energy (kWh)		90666	92505.6	94608	94082	91980	91192	91717	89352	93294	91980
Energy generated (kWh)		61800	63654	65563.6	67531	69556	71643	73792	76006	78286.4	80635
Demand (kWh)	60000	61800	63654	65563.6	67531	69556	71643	73792	76006	78286.4	80635
Energy to be sold without losses (kWh)		61231.4	63068.4	64960.4	66909	68917	70984	73114	75307	77566.2	79893.1
Receipts ($)	0	6609.57	7012.09	7439.13	7892.2	8372.8	8882.7	9423.7	9997.6	10606.4	11252.3
Investments ($)	37185										
Fix costs ($)	400	400	400	400	400	400	400	400	400	400	400
Energy losses (kWh)		568.56	585.617	603.185	621.28	639.92	659.12	678.89	699.26	720.235	741.842
Variable costs (energy losses) ($)		61.3726	65.1102	69.0754	73.282	77.745	82.48	87.503	92.832	98.4851	104.483
Total payments	37185	461.373	465.11	469.075	473.28	477.75	482.48	487.5	492.83	498.485	504.483
Cash flow ($)	-37185	6148.19	6546.98	6970.05	7418.9	7895.1	8400.2	8936.2	9504.7	10107.9	10747.9
Acumulated Cash flow ($)	-37185	-31037	-24490	-17520	-10101	-2205.8	6194.4	15131	24635	34743.2	45491.1
Actualized cash flow ($)	-37185	5800.18	5826.79	5852.19	5876.5	5899.6	5921.8	5943.1	5963.4	5982.87	6001.55
Acumulated actualized cash flow ($)	-37185	-31385	-25558	-19706	-13829	-7929.7	-2007.9	3935.1	9898.5	15881.4	21882.9

Conclusions

A complete DC voltage droop design has been presented that considers different dynamics of the DC microgrid. This methodology is based on a linearized model of the complete system. Design examples for the other loops in the system are presented (current loop, power loop and voltage loop). Based on the linearized model, advance control techniques are applied to determine the best droop constants to ensure that performance requirements are met (maximum DC voltage deviation of 10% and a transient power of maximum 10% over the converters nominal power). Then, the design procedure is validated through simulations of a three terminal DC microgrid where a solar plant is connected to the grid through two different buses.

Simulation results show an adequate response of the system to the power step change in the solar plant (representing the intermittent nature of solar radiation). DC voltages are kept withing the specified limits. Linear and non linear models have similar dynamics, confirming that the linear model is suitable for droop design. This design process can be applied to any DC microgrid configuration, with minor changes in the linear model and tunning process.

All simulations have been performed in Matlab/Simulink. Large and complex linear and non linear models where created making the simulation process long and with many errors till reaching the final and stable form. The droop controllers have been tuned using an integrated tool in Simulink Library called system tuner. This tool has many options regarding the tunning process, so finding the right setting was a time consuming process. The battery model was not included in the simulation. Simulation errors occurred when implementing the battery model. Since the focus of the thesis is the control strategy, the battery model was kept aside for future work. For more confirmation of the design process, a second simulation was attempted with a four terminal DC microgrid (two solar plants are connected to two different buses in the grid and interconnected between them) but with no success so far.

Future work implies a fault analysis of the system. When one of the converters becomes unavailable, all the power will be sent through the other converter. It is interesting to see how the system behaves in such a scenario. Also other microgrid configurations with different distributed generation elements (such as batteries) are to be analyzed. Different elements affect the system in a different way.

The work in this thesis has been validated through a paper developed in collaboration with Eduardo Prieto-Araujo, Enric Sánchez-Sánchez and Oriol Gomis-Bellmunt. The paper is called "Design methodology of the primary droop voltage control for DC microgrids" and it has been accepted for 2017 IEEE International Conference on DC Microgrids (ICDCM).

Thanks

I would like to thank my parents for their continuous support and making everything in their power, for me to reach this point. I would not be here without them.

Last but not least, I want to thank my coordinator, Eduardo Prieto Araujo, for the opportunity to contribute on my first, accepted and soon to be published, paper and for his advices that had a large impact on the quality of my work.

Doru Bogdan Bolboceanu
Barcelona, Spain
June 2017

References

[1] *Transition Energy*. URL: http://www.altenergy.org/transition/transition.html.

[2] John Nikoletatos and Stathis Tselepis. *Renewable Energy Integration in Power Grids*. Technology Brief. IEA-ETSAP and IRENA, 2015.

[3] Tom Morley. *Best Green Energy Choices for Your Home*. 2016. URL: http://www.greenpower-technology.co.uk/news-and-advice/best-green-energy-choices-home/.

[4] Paul Savage, Robert R. Nordhaus, and Sean P. Jamieson. *DC Microgrids: Benefits and Barriers*.

[5] A. Kwasinski. "Quantitative Evaluation of DC Microgrids Availability: Effects of System Architecture and Converter Topology Design Choices". In: *IEEE Transactions on Power Electronics* 26.3 (2011), pp. 835–851. ISSN: 0885-8993. DOI: 10.1109/TPEL.2010.2102774.

[6] H. Ikebe. "Power systems for telecommunications in the IT age". In: *Proc. INTELEC* (2003), pp. 1–8.

[7] Stephen Whaite, Brandon Grainger, and Alexis Kwasinski. "Power Quality in DC Power Distribution Systems and Microgrids". In: *Energies* (2015), pp. 4378–4398. ISSN: 1996-1073.

[8] Agustí Egea-Alvarez, Adrià Junyent-Ferré, and Oriol Gomis-Bellmunt. *Active and reactive power control of grid connected distributed generation systems*. CITCEA-UPC.

[9] Marta Bobis Uría. "Operation and Control of Multi-Terminal DC (MTDC) Grids". Master Thesis. Aalborg: Aalborg University, June 2013, pp. 19–22.

[10] Ulrich Boeke and Matthias Wendt. "Comparison of low voltage AC and DC power grids". In: *Philips Research* ().

[11] A. Bellini et al. "Simplified model of a photovoltaic module". In: *2009 Applied Electronics*. 2009, pp. 47–51.

[12] N. Hamrouni and A. Chérif. "Modelling and control of a grid connected photovoltaic system". In: ().

[13] D. Sera, R. Teodorescu, and P. Rodriguez. "PV panel model based on datasheet values". In: *2007 IEEE International Symposium on Industrial Electronics*. 2007, pp. 2392–2396. DOI: 10.1109/ISIE.2007.4374981.

[14] Naoki Ayai et al. "DC Micro Grid System". In: *ELECTRIC WIRE CABLE, ENERGY* ().

[15] Min Chen and G. A. Rincon-Mora. "Accurate electrical battery model capable of predicting runtime and I-V performance". In: *IEEE Transactions on Energy Conversion* 21.2 (2006), pp. 504–511. ISSN: 0885-8969. DOI: 10.1109/TEC.2006.874229.

[16] Gunnar Asplund, Kjell Eriksson, and Kjell Svensson. “DC Transmission based on Voltage Source Converters”. In: *CIGRE SC14 Colloquium in South Africa 1997*. Ed. by ABB Power Systems AB. 1997.

[17] Ned Mohan, Tore M. Undeland, and William P. Robbins. *Power Electronics. Converters, Applications and Design*. third. John Wiley and Sons, Inc, 2003.

[18] S. Akkari et al. “Impact of the DC cable models on the SVD analysis of a Multi-Terminal HVDC system”. In: *2016 Power Systems Computation Conference (PSCC)*. 2016, pp. 1–6. DOI: 10.1109/PSCC.2016.7541034.

[19] Catalin Gavriluta. “Control and Operation of Multi-Terminal VSC-DC Networks”. PhD Thesis. Universitat Politecnica de Catalunya, 2014.

[20] Lennart Söder and Mikael Amelin. *Efficient Operation and Planning of Power Systems*. course compendium. Version 11. Stockholm: Royal Institute of Technology, 2011, pp. 35–40.

[21] E. Prieto-Araujo et al. “DC Voltage Droop Control Design for Multiterminal HVDC Systems Considering AC and DC Grid Dynamics”. In: *IEEE Transactions on Power Delivery* 31.2 (2016), pp. 575–585. ISSN: 0885-8977. DOI: 10.1109/TPWRD.2015.2451531.

[22] Ahmed Mohamed. “Hierarchical Control for DC Microgrids, Energy Management of Distributed Generation Systems”. In: *InTech* (2016). Ed. by Associate Prof. Lucian Mihet-Popa.

[23] Chin-Hsing Cheng. “Implementation of a Small Type DC Microgrid Based on Fuzzy Control and Dynamic Programming”. In: *Energies* (2014). Ed. by Chunhua Liu. DOI: 10.3390/9100781.

[24] Meng Lexuan et al. “Agent-based distributed hierarchical control of dc microgrid systems”. In: *Proceedings of Electrimacs 2014* (2014), pp. 281–286.

[25] Eduardo Prieto-Araujo et al. “Design methodology of the primary droop voltage control for DC microgrids”. In: (2017).

[26] Sigurd Skogestad and Ian Postlethwaite. *Multivariable Feedback Control: Analysis and Design*. John Wiley & Sons, 2005. ISBN: 0470011688.

[27] *H-infinity methods in control theory*. 2017. URL: https://en.wikipedia.org/wiki/H-infinity_methods_in_control_theory.

[28] U.S. Department of Energy, ed. *Average Retail Prices of Electricity, 1960-2011*. 2012. URL: https://www.eia.gov/totalenergy/data/annual/showtext.php?t=ptb0810.

[29] U.S. Department of Energy, ed. *Average Price of Electricity to Ultimate Customers by End-Use Sector*. 2017. URL: https://www.eia.gov/electricity/monthly/epm_table_grapher.php?t=epmt_5_6_a.

[30] Ran Fu et al. *U.S. Solar Photovoltaic System Cost Benchmark: Q1 2016*. report. NREL, Sept. 2016. ISRN: PR-6A20-67142.

[31] www.industrialextensionleads.co.uk, ed. *10m 400v 3 phase 5 pin 32a extension lead (6mm H07 cable) IP44 Rated*. URL: https://www.industrialextensionlea
co.uk/10m--400v-3-phase-5-pin--32a-extension-lead-6mm-h07-cable-ip44-rated-9569-p.asp.

[32] www.platt.com, ed. *Acme T3030K0013B Transformer, Dry Type, NEMA 3R, DOE 2016, 480 x 208Y/120*. URL: https://www.platt.com/platt-electric-supply/Dry-Type-Transformers-480-208Y-120-150C-Rise/Acme/T3030K0013B/product.aspx?zpid=184713.

[33] www.urjakart.com, ed. *Polycab 4 sq. mm Solar Copper DC Cable*. URL: http://www.urjakart.com/polycab-4-sq-mm-solar-copper-dc-cable.html.

[34] National Renewable Energy Laboratory (U.S.) et al. *Comparative Study of DC and AC Microgrids in Commercial Buildings Across Different Climates and Operating Profiles*. United States. Department of Energy. Office of Energy Efficiency and Renewable Energy, 2015. URL: https://books.google.es/books?id=1YegnQAACAAJ.

[35] Francisco Díaz-González. "Cost-Benefit Analysis Workshop". May 2017.

[36] P. Mattavelli and F. P. Marafao. "Repetitive-based control for selective harmonic compensation in active power filters". In: *IEEE Transactions on Industrial Electronics* 51.5 (2004), pp. 1018–1024. ISSN: 0278-0046. DOI: 10.1109/TIE.2004.834961.

A. Appendix

A.1 Clarke Transformation

In electrical engineering, Clarke transformation (also known as $\alpha\beta0$ transformation) is a mathematical procedure to transform three phase quantities (*abc* reference) into $\alpha\beta0$ orthogonal reference frame. This procedure is used to simplify three-phase circuits analysis. The transformation is defined as:

$$[x_{\alpha\beta0}] = [T_{\alpha\beta0}][x_{abc}] \tag{A.1}$$

The inverse transformation is defined as:

$$[x_{abc}] = [T_{\alpha\beta0}]^{-1}[x_{\alpha\beta0}] \tag{A.2}$$

where x_{abc} contains quantities (currents or voltages) in *abc* reference frame, $x_{\alpha\beta0}$ contains quantities in $\alpha\beta0$ reference frame and $T_{\alpha\beta0}$ is the transformation matrix.

A geometric representation of Clarke transformation is shown in Fig

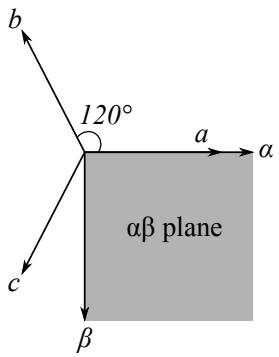

Figure A.1: $\alpha\beta0$ geometric representation

In a more explicit way, equations equations A.1 and A.2 can be expressed as:

$$\begin{bmatrix} x_\alpha \\ x_\beta \\ x_0 \end{bmatrix} = \frac{2}{3}\begin{bmatrix} 1 & -\frac{1}{2} & -\frac{1}{2} \\ 0 & -\frac{\sqrt{3}}{2} & \frac{\sqrt{3}}{2} \\ \frac{1}{2} & \frac{1}{2} & \frac{1}{2} \end{bmatrix}\begin{bmatrix} x_a \\ x_b \\ x_c \end{bmatrix} \tag{A.3}$$

$$\begin{bmatrix} x_a \\ x_b \\ x_c \end{bmatrix} = \begin{bmatrix} 1 & 0 & 1 \\ -\frac{1}{2} & -\frac{\sqrt{3}}{2} & 1 \\ -\frac{1}{2} & \frac{\sqrt{3}}{2} & 1 \end{bmatrix}\begin{bmatrix} x_\alpha \\ x_\beta \\ x_0 \end{bmatrix} \tag{A.4}$$

If we express this variables as voltages for example, they would look like:

A.2 Park Transformation

Even though $\alpha\beta0$ has benefits in lots of applications, for designing controllers it is more useful to use constant quantities (or *dq* quantities). They are obtained using

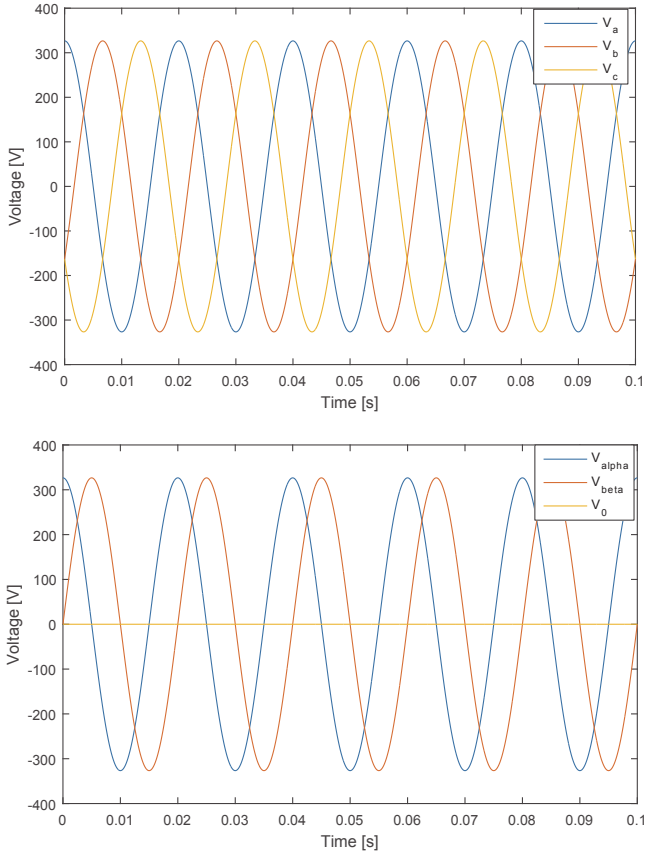

Figure A.2: Voltages in *abc* and $\alpha\beta$ references

Park transformation as explained bellow:

$$[x_{dq0}] = [T_{dq0}][x_{abc}] \tag{A.5}$$

The inverse transformation is obtained from:

$$[x_{abc}] = [T_{dq0}]^{-1}[x_{dq0}] \tag{A.6}$$

where x_{abc} contains *abc* variables, x_{dq0} contains dq variables and T_{dq0} is Park transformation matrix.

A geometric representation of the Park transformation can be seen in Fig.

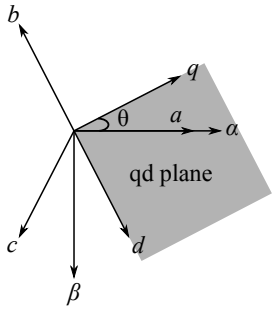

Figure A.3: dq geometric representation

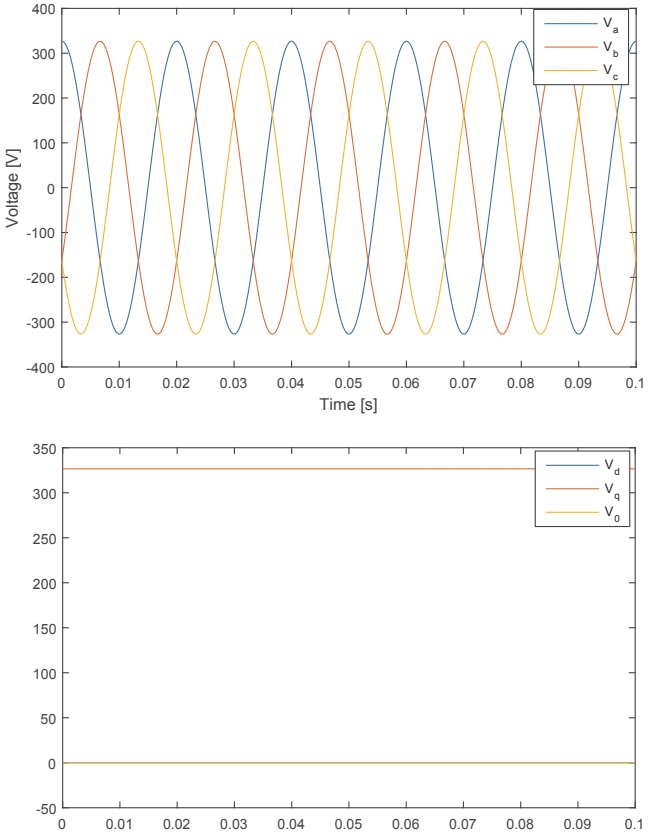

Figure A.4: Voltages in *abc* and *dq*0 references

In a more explicit way, equations xx and xx can be written as:

$$\begin{bmatrix} x_d \\ x_q \\ x_0 \end{bmatrix} = \frac{2}{3} \begin{bmatrix} \cos(\theta) & \cos(\theta - \frac{2\pi}{3}) & \cos(\theta + \frac{2\pi}{3}) \\ \sin(\theta) & \sin(\theta - \frac{2\pi}{3}) & \sin(\theta + \frac{2\pi}{3}) \\ \frac{1}{2} & \frac{1}{2} & \frac{1}{2} \end{bmatrix} \begin{bmatrix} x_a \\ x_b \\ x_c \end{bmatrix} \tag{A.7}$$

$$\begin{bmatrix} x_a \\ x_b \\ x_c \end{bmatrix} = \begin{bmatrix} \cos(\theta) & \sin(\theta) & 1 \\ \cos(\theta - \frac{2\pi}{3}) & \sin(\theta - \frac{2\pi}{3}) & 1 \\ \cos(\theta + \frac{2\pi}{3}) & \sin(\theta + \frac{2\pi}{3}) & 1 \end{bmatrix} \begin{bmatrix} x_d \\ x_q \\ x_0 \end{bmatrix} \tag{A.8}$$

If we express these variables as voltages they would look like:

A.3 Singular Value Decomposition

A matrix is considered a unitary matrix if:

$$U^T = U^{-1} \tag{A.9}$$

All eigenvalues for unitary matrix have an absolute value of 1 and all the singular values are 1.

Any matrix A with the size $m \times n$ can be transformed into a singular value decomposition as :

$$A = U\Sigma V^T \tag{A.10}$$

where U and V are unitary matrices with the size $l \times l$ and $m \times m$ and Σ is a diagonal matrix that contains non-negative singular values, σ_i arranged in descending order[26]:

$$\Sigma = \begin{bmatrix} \Sigma_1 \\ 0 \end{bmatrix}; \quad l \geqslant m \tag{A.11}$$

or

$$\Sigma = \begin{bmatrix} \Sigma_1 & 0 \end{bmatrix}; \quad m \geqslant l \tag{A.12}$$

where

$$\Sigma_1 = \text{diag}\{\sigma_1, \sigma_2, ..., \sigma_k\}; \quad k = \min(l, m) \tag{A.13}$$

and

$$\sigma_k \geqslant, ..., \geqslant \sigma_2 \geqslant \sigma_1 \tag{A.14}$$

The column vectors of V are called input singular vectors and the column vectors of U are called are called output singular vectors. The singular values are positive square roots of the largest eigenvalue of AA^T and A^TA, defined as:

$$\sigma_i(A) = \sqrt{\lambda_i(A^TA)} = \sqrt{\lambda_i(AA^T)} \tag{A.15}$$